Elliptical Galaxies,

Triaxial Potential

Schwarzschild Modelling

bulge
gas-free (largely)
old stars

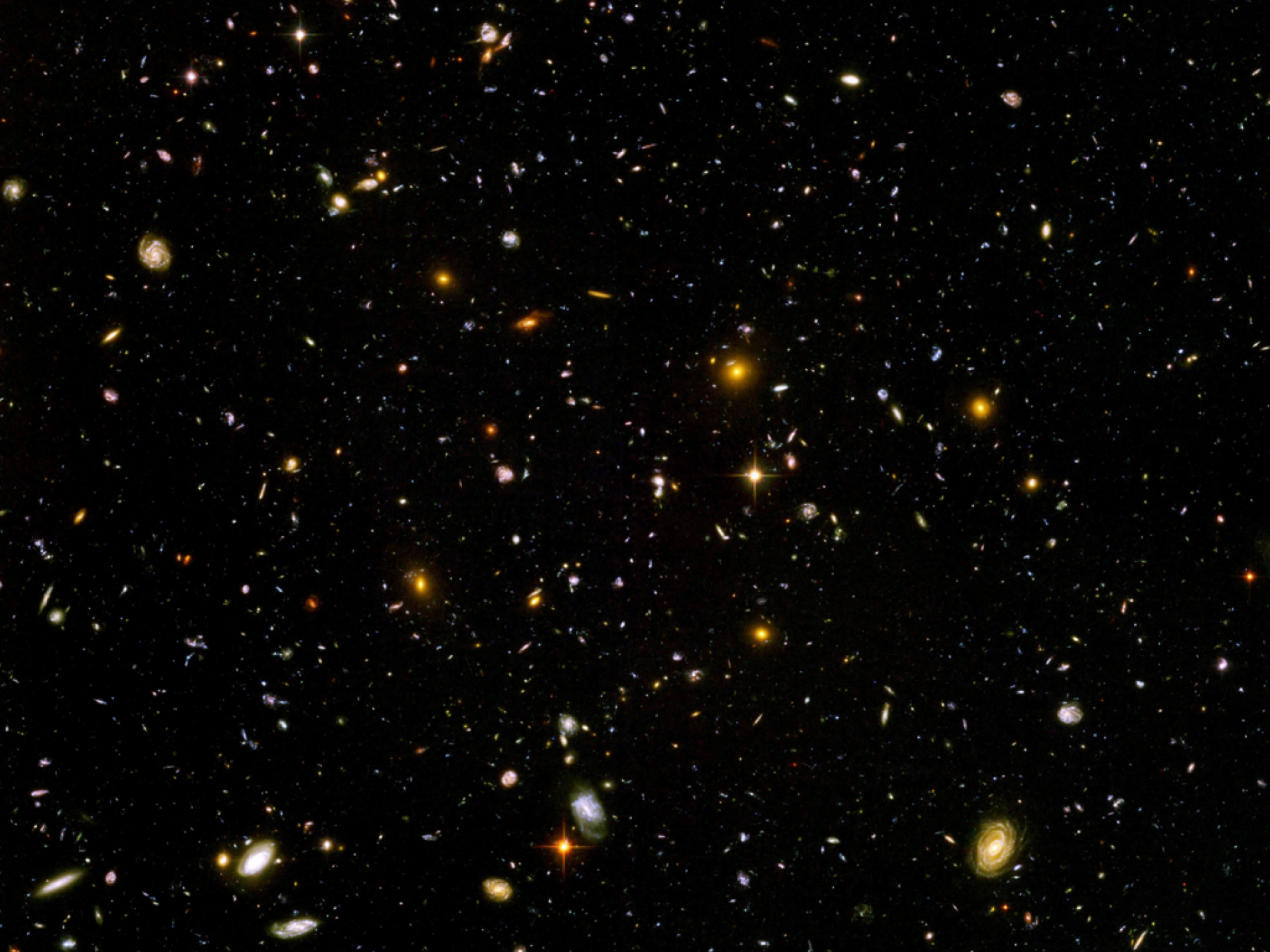

(a) Two scenarios discussed

(i) Monolithic Dissipative Collapse

- Early massive gas cloud undergoes dissipative collapse
- Huge starburst **during** collapse

  Note: sub-mm detections of ~10^{10} $M_\odot$ cold gas at z ~ 2-3 with high SFR.
- Clumpiness during collapse → violent relaxation → ~ isothermal

  incomplete violent relaxation → non-isothermal & non-isotripic
- Probably rotate "rapidly" → "Disky" Ellipticals ???

(ii) Hierarchical Mergers

- Early universe much denser: e.g. z ~ 2 density ~ 27 times higher than today.

  → Mergers/interactions probably common.
- Sequence of galactic mergers, starting with pre-galactic substructures
- Galaxies continuue to grow during z ~ 1-2

  Note : HST finds **old** ellipticals at z ~ 0.5
- Galaxies fall into clusters and merging ceases (encounter velocities too high)
- Random accretions → low AM & anisotropic → "Boxy" Ellipticals ???

reality likely a combination
but how do each process give rise to the observed correlations?

Elliptical galaxies have varying amount of rotation support.

Brighter ones have less. Flattened, but not by rotational flattening.

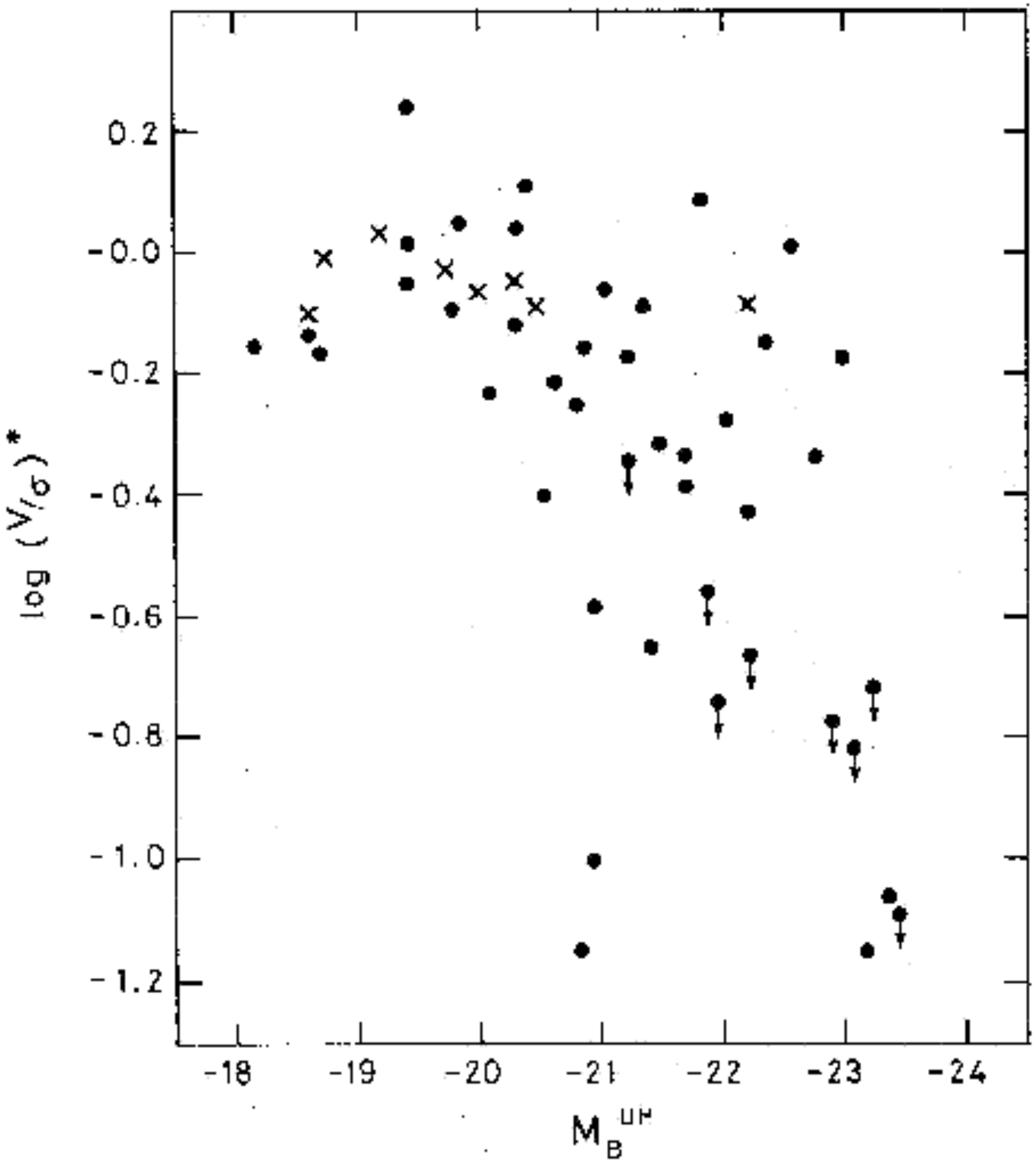

FIG. 4.—Log $(V/\sigma)^*$ against absolute magnitude. Ellipticals are shown as filled circles and the bulges as crosses; $(V/\sigma)^*$ is defined in § IIIb.

The **Sersic** profile is found to describe well the surface brightness profile for many ellipticals. Scale-length increasing with R.

$$I(R) = I_e \, exp\left(-b \left[(R/R_e)^{1/n} - 1 \right]\right)$$

spiral bulge: n=4 (de Vaucouleur's)
spiral disk: n=1

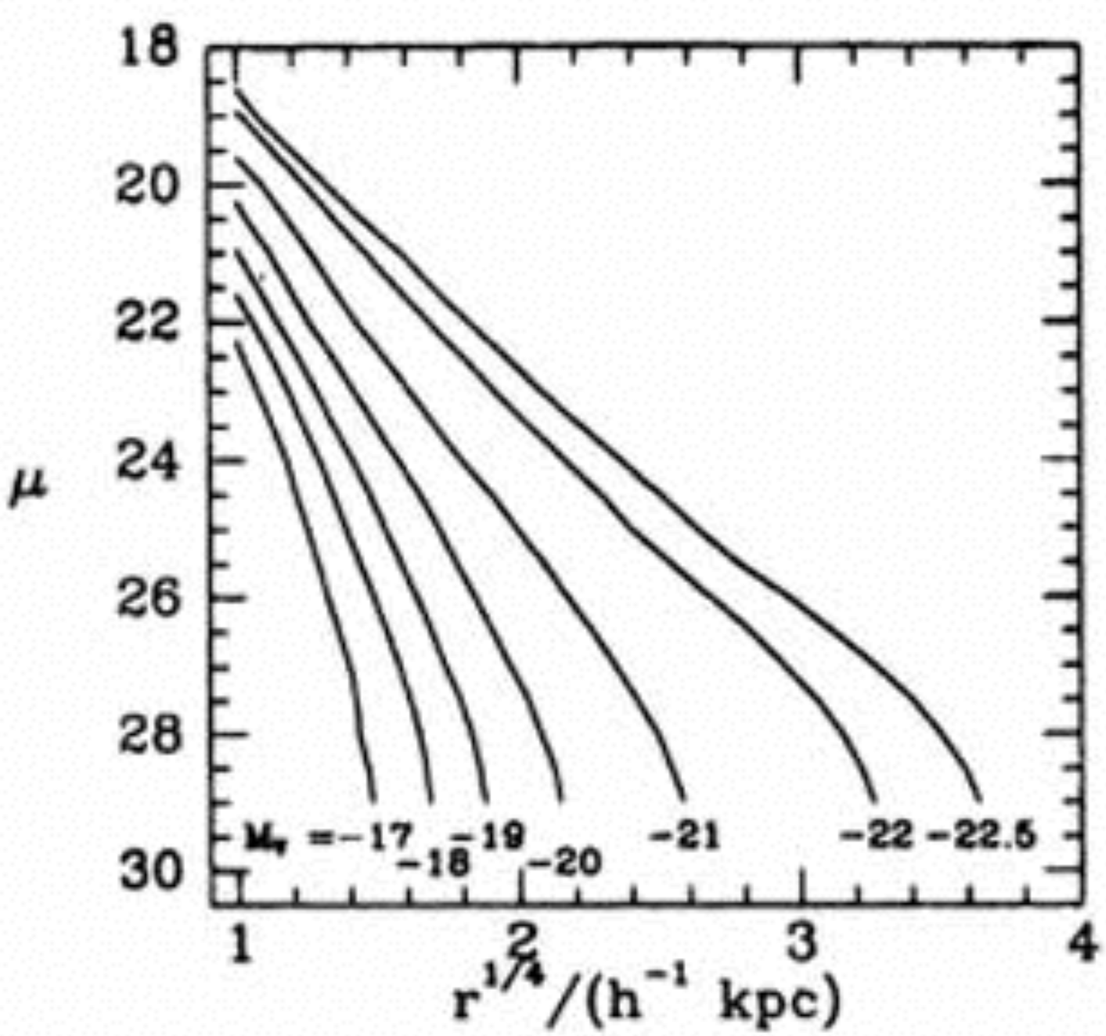

more luminous Elliptical galaxies have higher n-index (more centrally concentrated). Kormendy et al '06

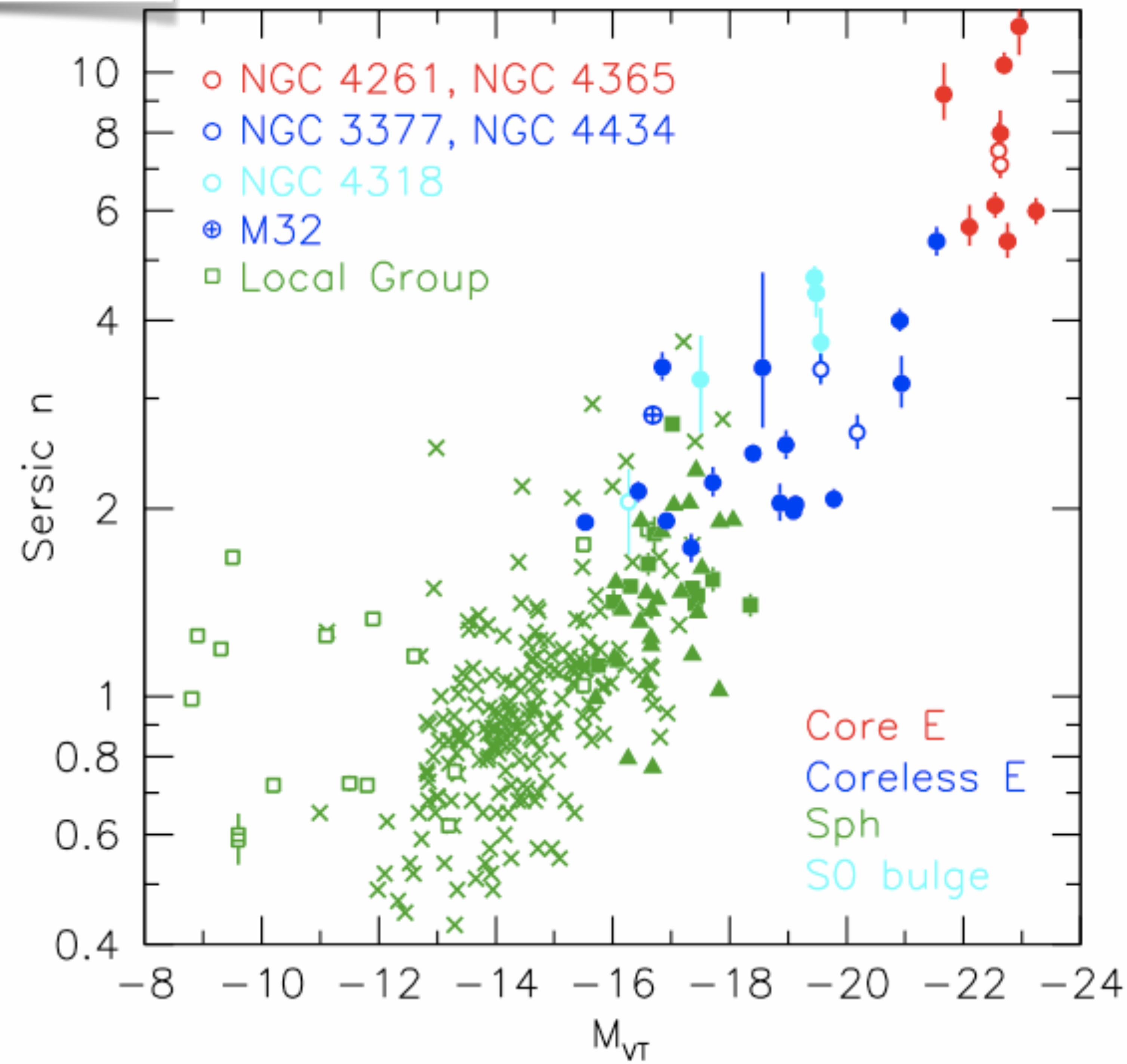

Inner region: Power-law vs. Cuspy Ellipticals

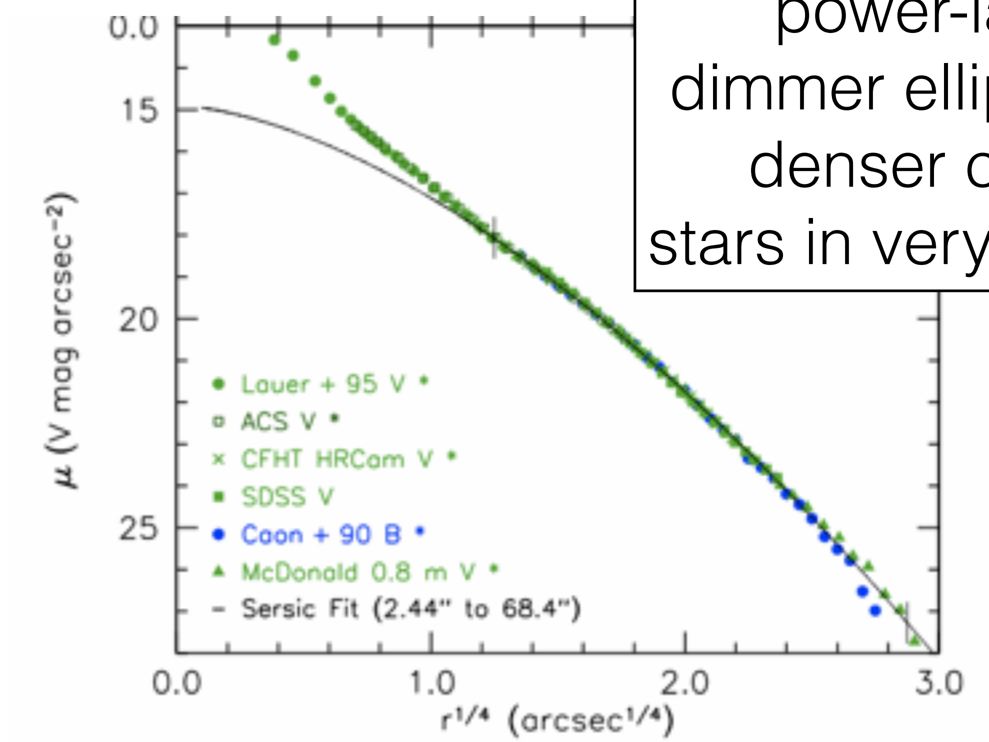

power-law
dimmer ellipticals
denser core
stars in very centre

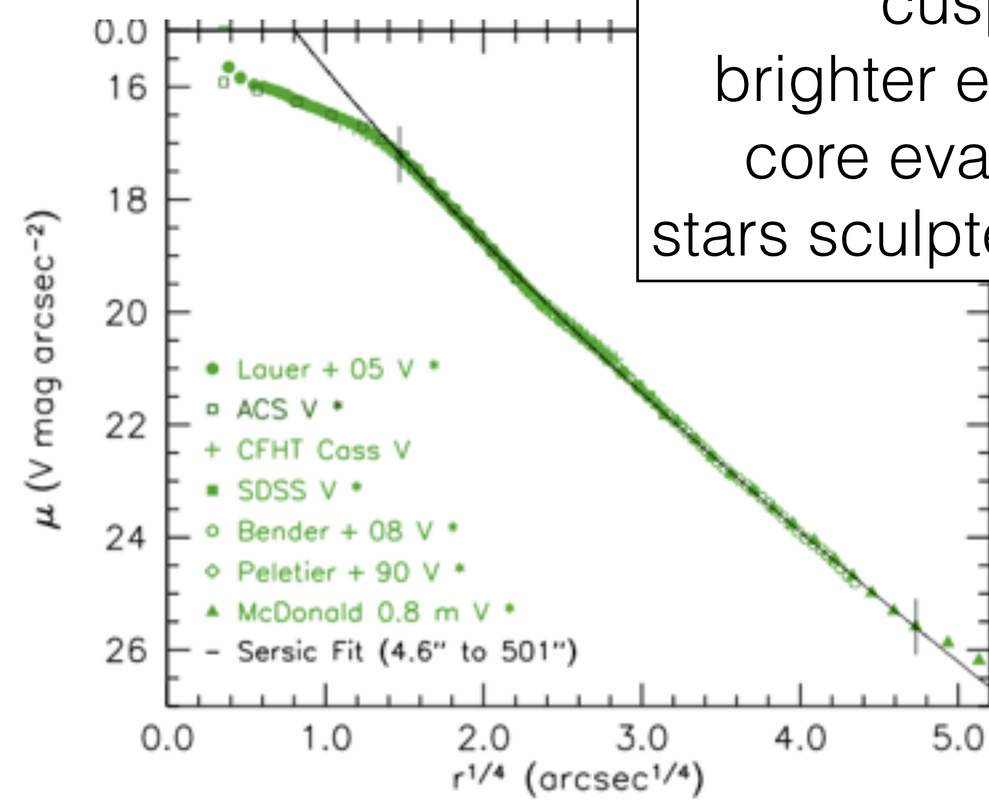

cuspy
brighter ellipticals
core evacuated
stars sculpted by BH?

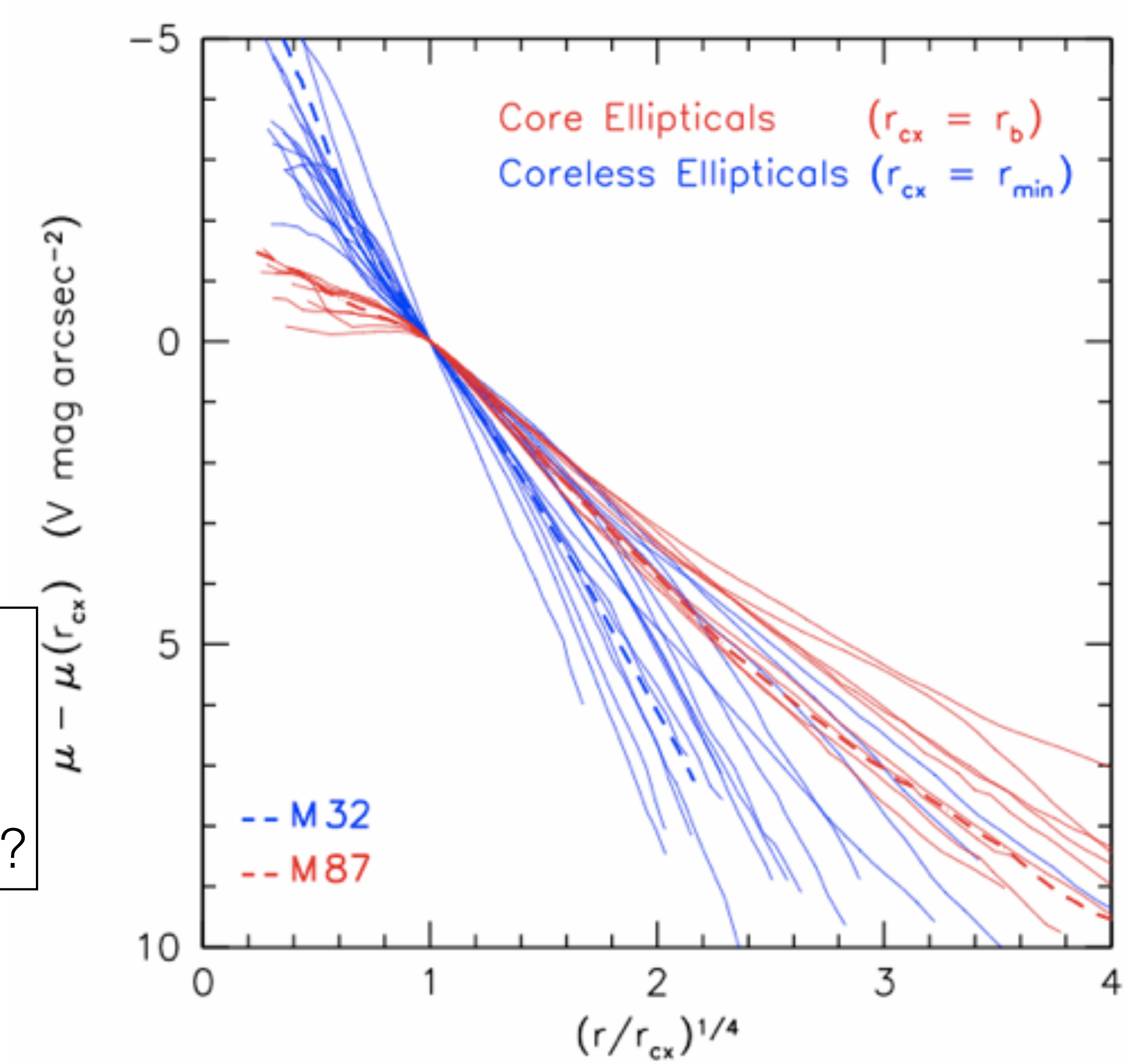

FIG. 40.— Major-axis profiles of all of our ellipticals scaled together to illustrate the dichotomy between core and coreless ellipticals. Core ellipticals are scaled together at $r_{cx} = r_b$, the break radius given by the Nuker function fit in Lauer et al. (2007b). Coreless ellipticals are scaled together at the minimum radius r_{min} that was used in our Sérsic fits; interior to this radius, the profile is dominated by extra light above the inward extrapolation of the outer Sérsic fit.

Faber-Jackson relation: more luminous ellipticals have deeper potentials

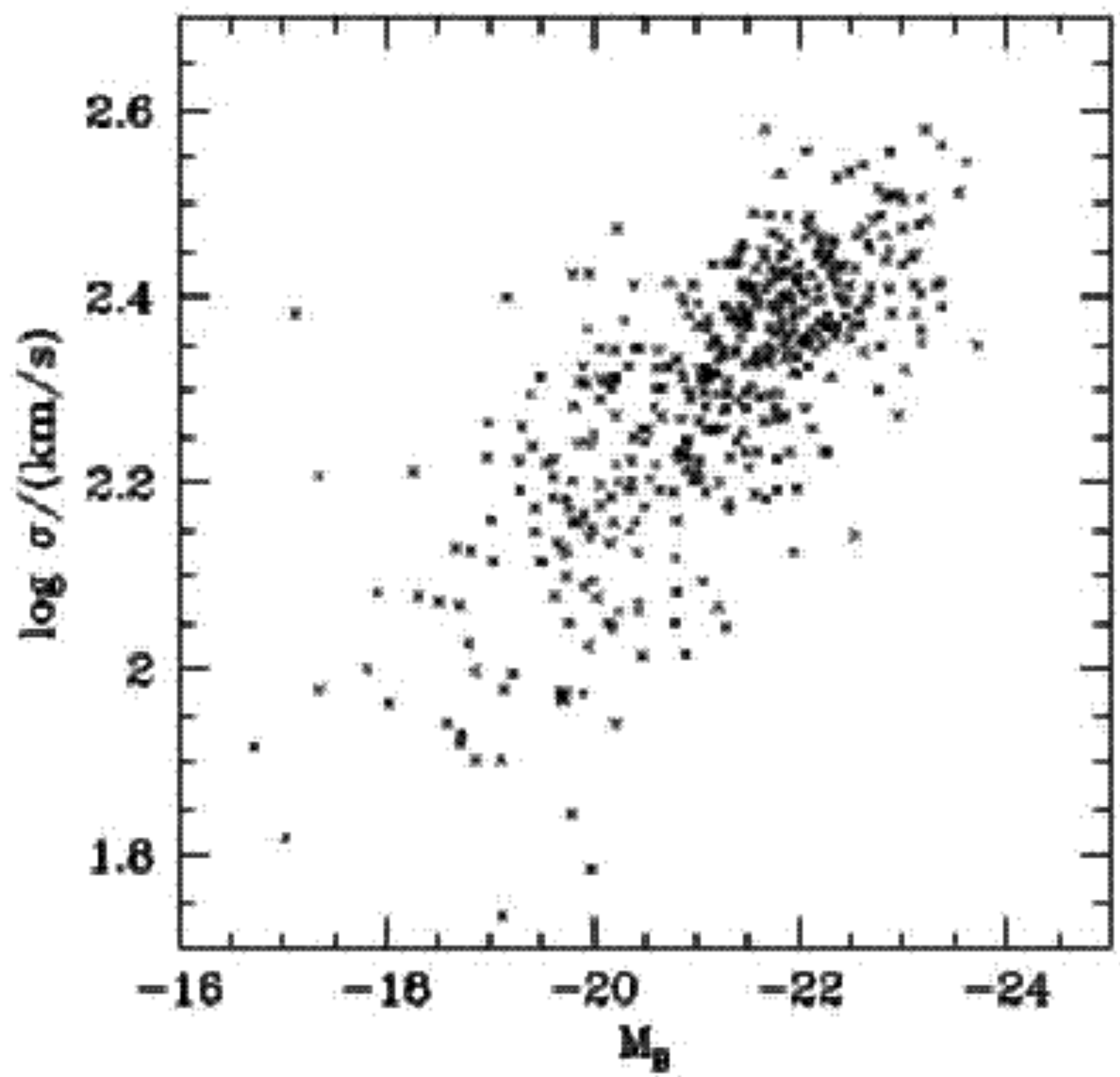

Faber-Jackson relation between central velocity dispersion and total magnitude of elliptical galaxies

$$\boxed{L_B \propto \sigma^4}$$

Ellipticals are likely triaxial bodies: a > b > c

$$\frac{x^2}{a^2} + \frac{y^2}{b^2} + \frac{z^2}{c^2} = r^2$$

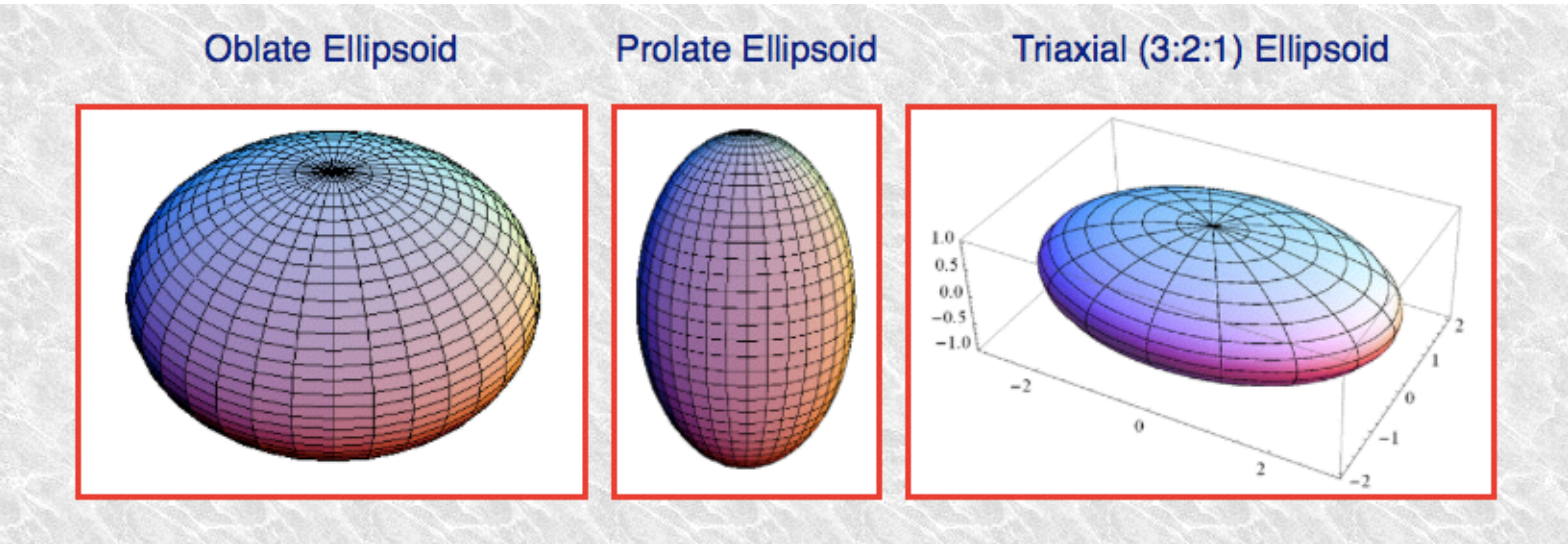

. systems that are rotationally supported likely axi-symmetric (a=b); rotation around short-axis (c)
. but systems supported by velocity dispersion do not have to be (imagine superimposing two oblique rotating disks).

$$\frac{x^2}{a^2} + \frac{y^2}{b^2} + \frac{z^2}{c^2} = r^2$$

if population triaxial
a:b:c=1:0.98:0.68

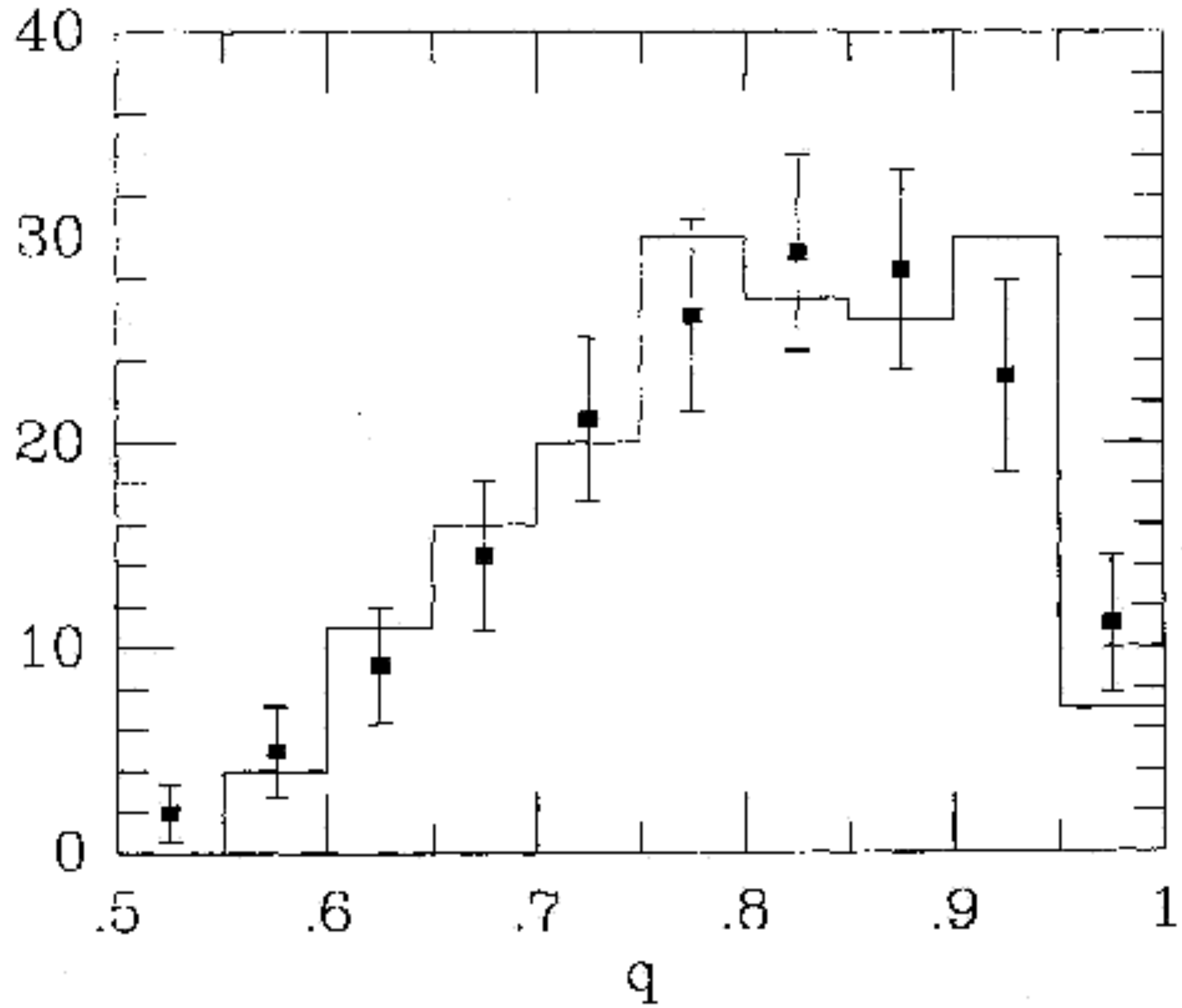

FIG. 6.—Binned distribution functions of apparent axis ratios. The histogram gives the apparent axis ratios of the 171 elliptical galaxies in the observational sample. The points and error bars give the mean and standard deviation expected from a sample of 171 galaxies drawn from the Gaussian function $f(\beta, \gamma)$ with $\sigma_0 = 0.11$, $\beta_0 = 0.98$, and $\gamma_0 = 0.69$. The two functions have a reduced χ^2 score of $\chi^2/\nu = 1.2$.

see: Ryden (1992) *ApJ*, **396**, 445R

a,b,c functions of r
— twisted isophotes

Photometry can only go so far.

For real understanding, have to go to kinematics (spectroscopy)

1) individual stellar orbit
2) collection of stellar orbits

Orbits in a spherical potential stay in a plane.

$$\Phi = \Phi(r)$$

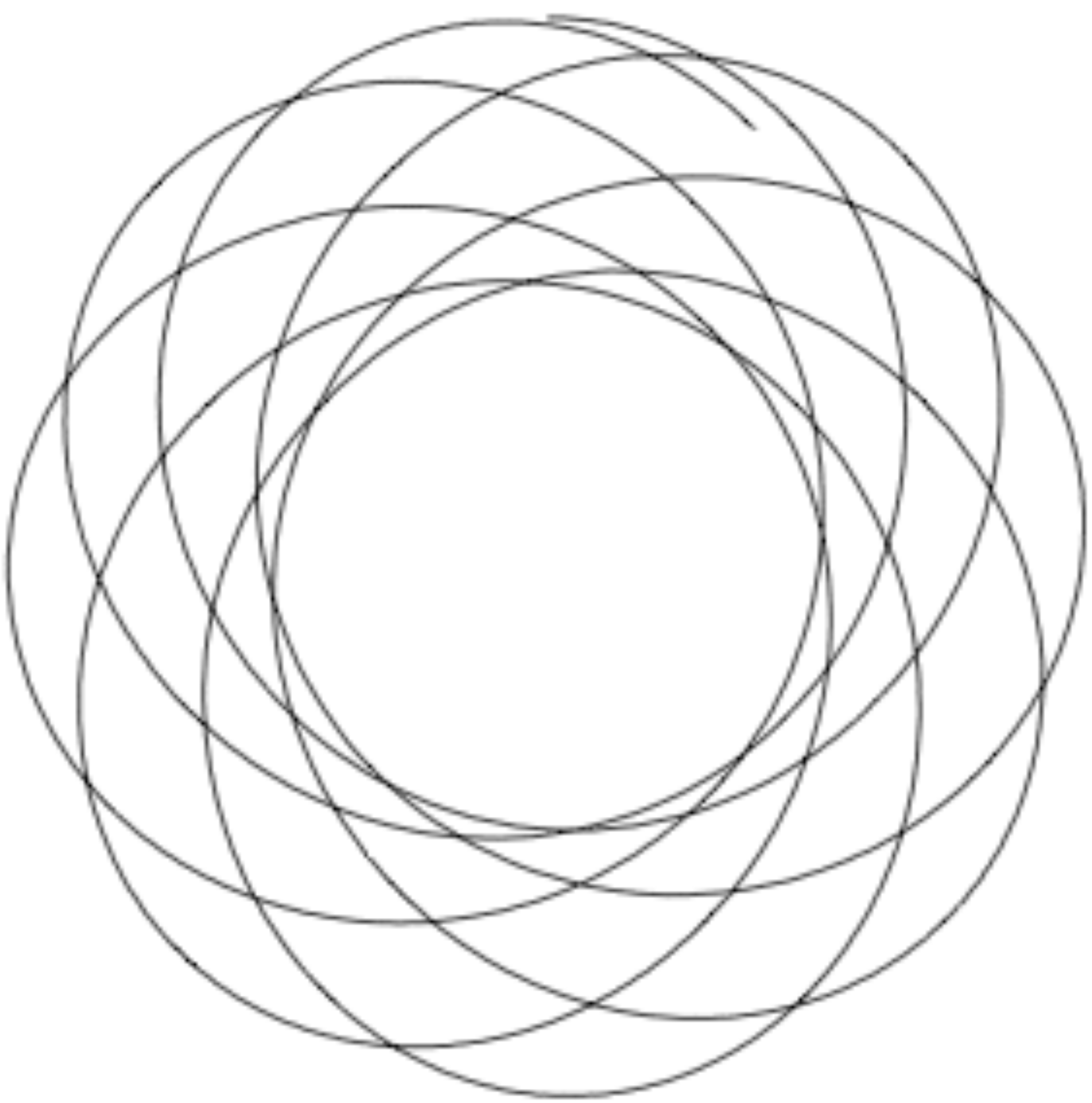

Figure 3.1 A typical orbit in a spherical potential (the isochrone, eq. 2.47) forms a rosette.

axi-symmetric potential

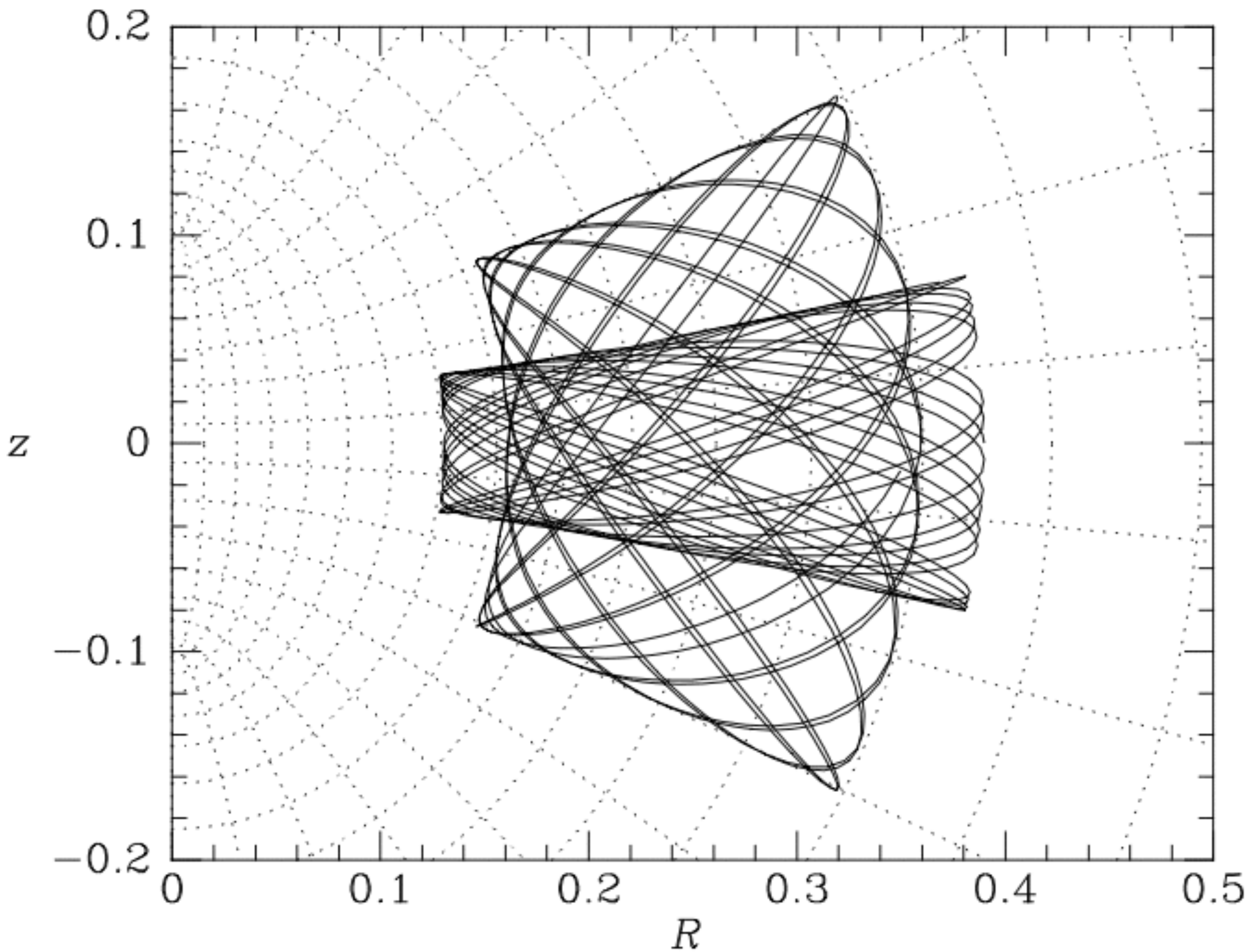

Figure 3.27 The boundaries of orbits in the meridional plane approximately coincide with the coordinate curves of a system of spheroidal coordinates. The dotted lines are the coordinate curves of the system defined by (3.242) and the full curves show the same orbits as Figure 3.4.

Axisymmetric potential: largely rotation supported; conserve Lz

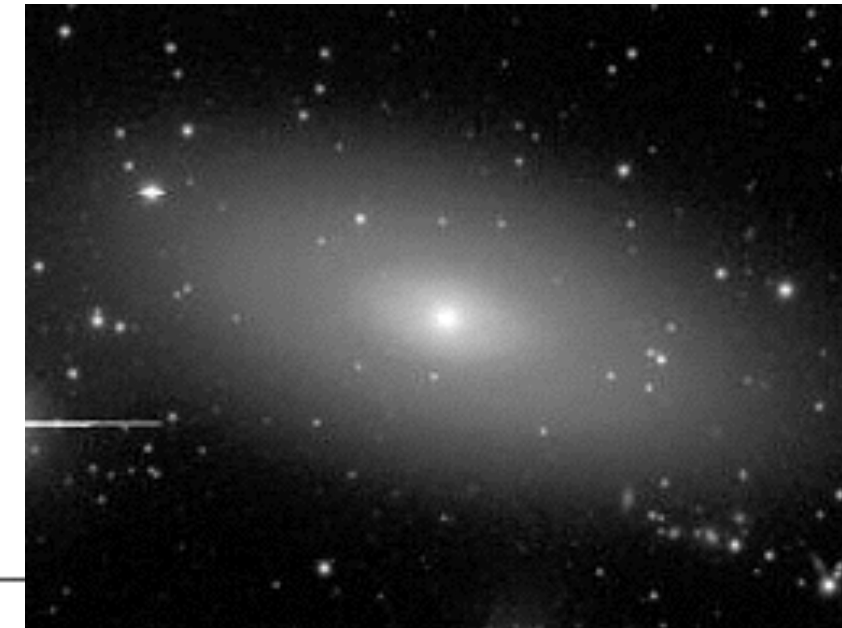

$$\Phi_{\rm eff} = \tfrac{1}{2} v_0^2 \ln\left(R^2 + \frac{z^2}{q^2}\right) + \frac{L_z^2}{2R^2}, \qquad (3.70)$$

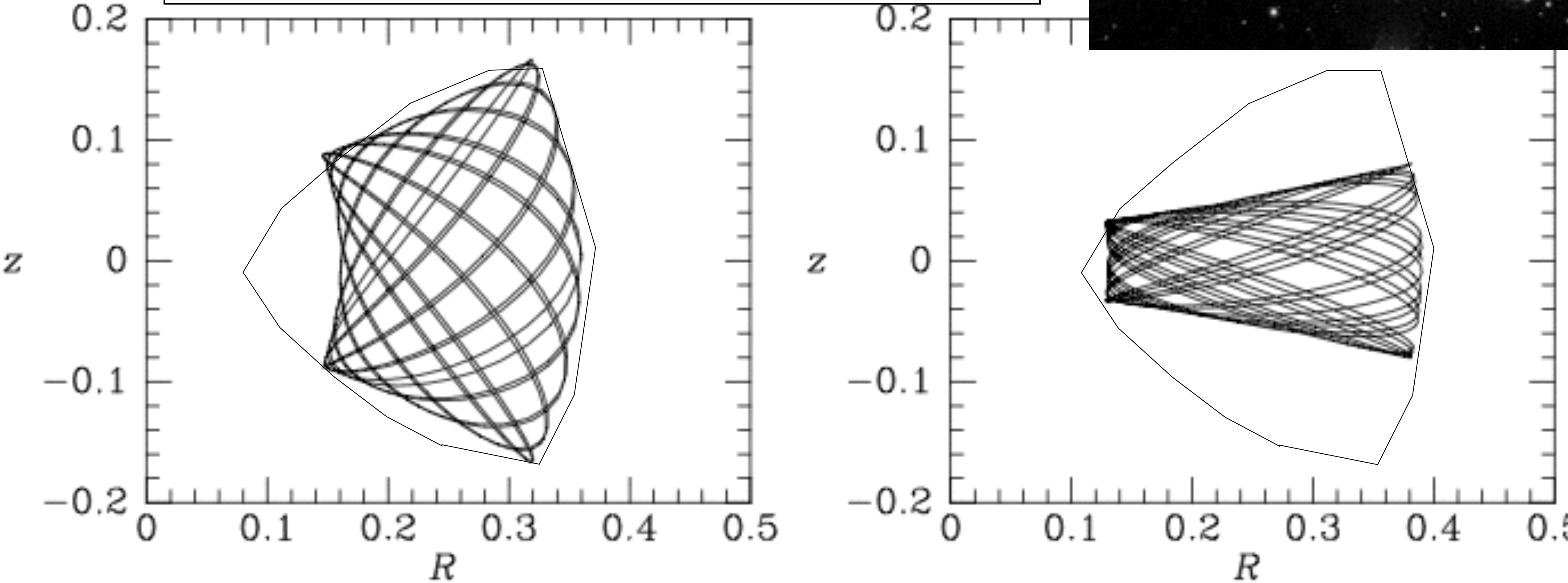

Figure 3.4 Two orbits in the potential of equation (3.70) with $q = 0.9$. Both orbits are at energy $E = -0.8$ and angular momentum $L_z = 0.2$, and we assume $v_0 = 1$.

. logarithmic potential gives rise to flat rotation curve
. gradual precession of the orbital plane
. space allowed by ZVC not filled up -- 3rd integral

Poincare surface of section (visualize 3-D orbit as a 1-D motion)

Jules Henri Poincaré (1854–1912). Photograph from the frontispiece of the 1913 edition of *Last Thoughts*.

strobe (**surface of section**)
e.g., when $z=0$, $p_z > 0$

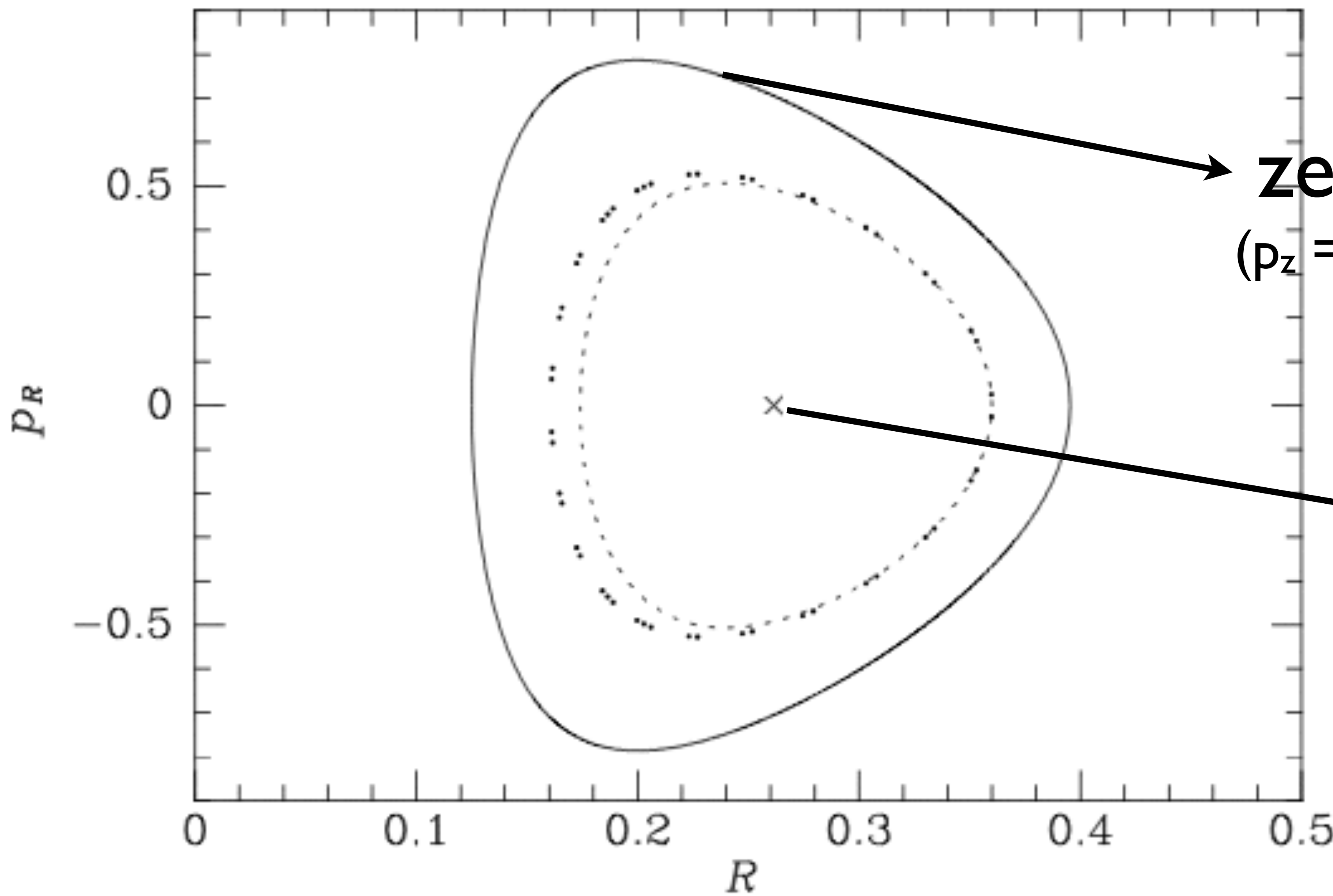

zero velocity curve
($p_z = 0$) — particle remains $z=0$

circular orbit
$p_R=0$, $p_z=0$

re 3.5 Points generated by the orbit of the left panel of Figure 3.4 in the (R, p_R) ce of section. If the total angular momentum L of the orbit were conserved, the points d fall on the dashed curve. The full curve is the zero-velocity curve at the energy of orbit. The × marks the consequent of the shell orbit.

Orbits in Non-axisymmetric potential

$$\Phi = \Phi(x, y, z)$$

first consider: planar potential (2-D, no z-direction)

Logarithmic potential (2-D)

$$\Phi_{\mathrm{L}}(x, y) = \tfrac{1}{2} v_0^2 \ln\left(R_{\mathrm{c}}^2 + x^2 + \frac{y^2}{q^2}\right) \quad (0 < q \leq 1). \qquad (3.103)$$

centre-philic, box orbit

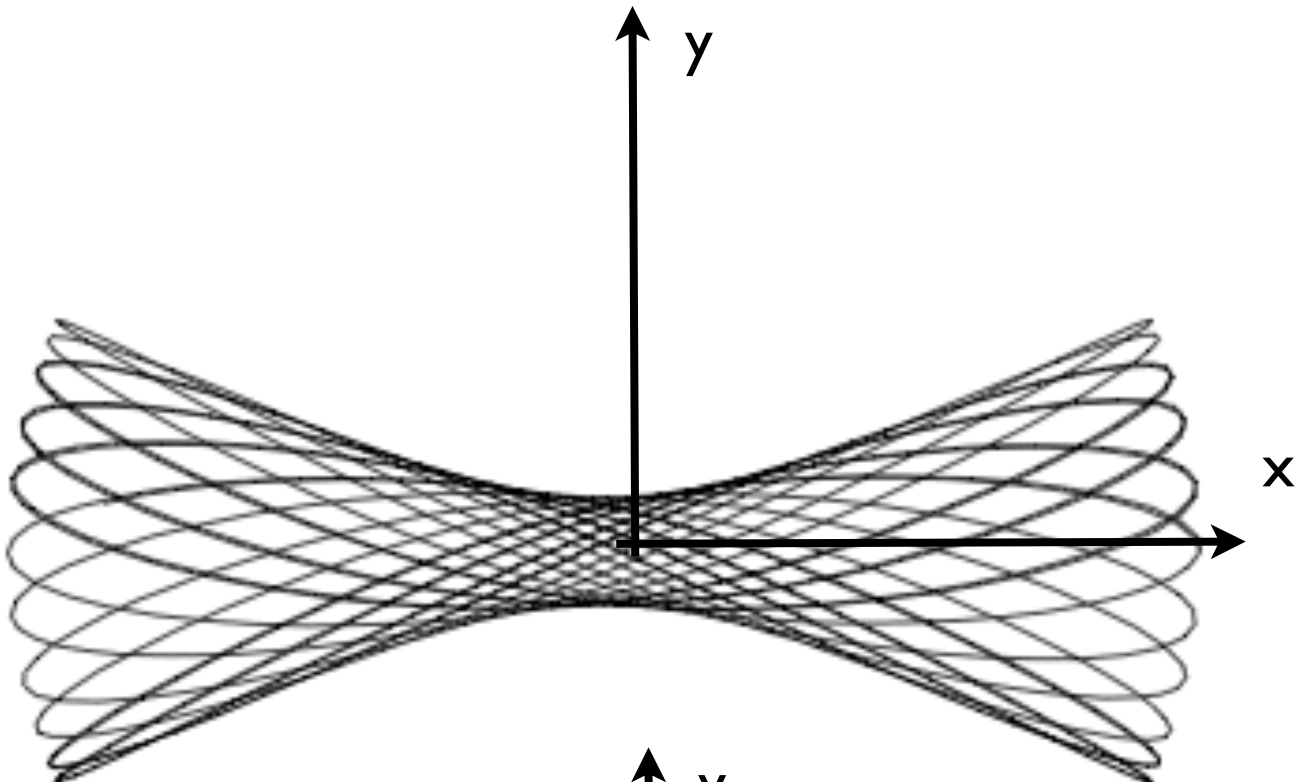

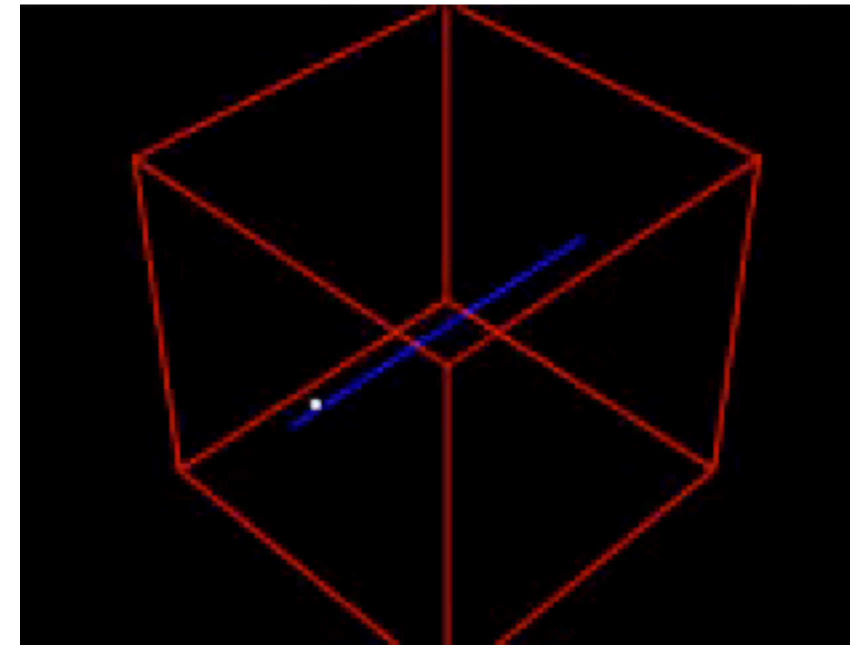

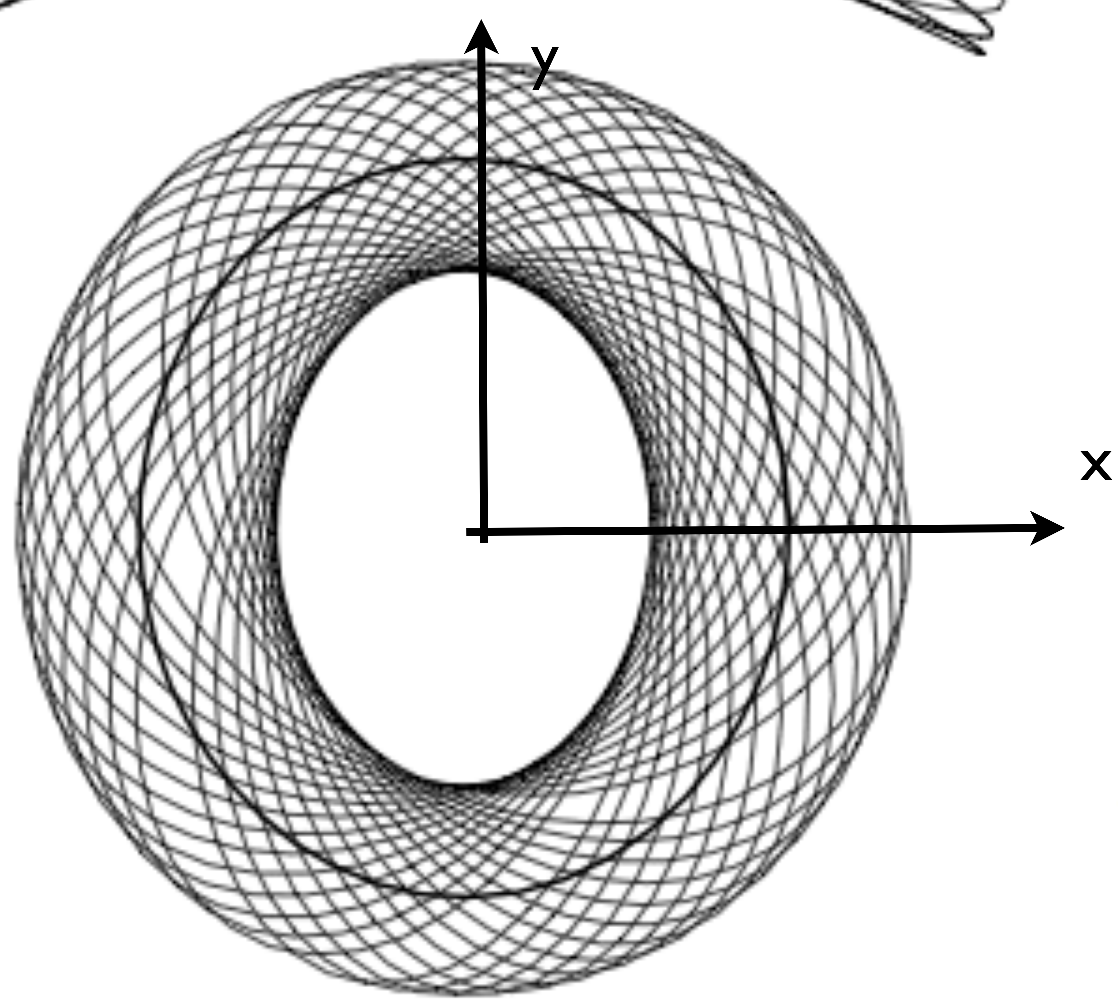

Figure 3.8 Two orbits of a common energy in the potential Φ_L of equation (3.103) when $v_0 = 1$, $q = 0.9$ and $R_{...}$
orbit; bottom,
closed parent o
shown. The en
that of the isop
cuts the long a

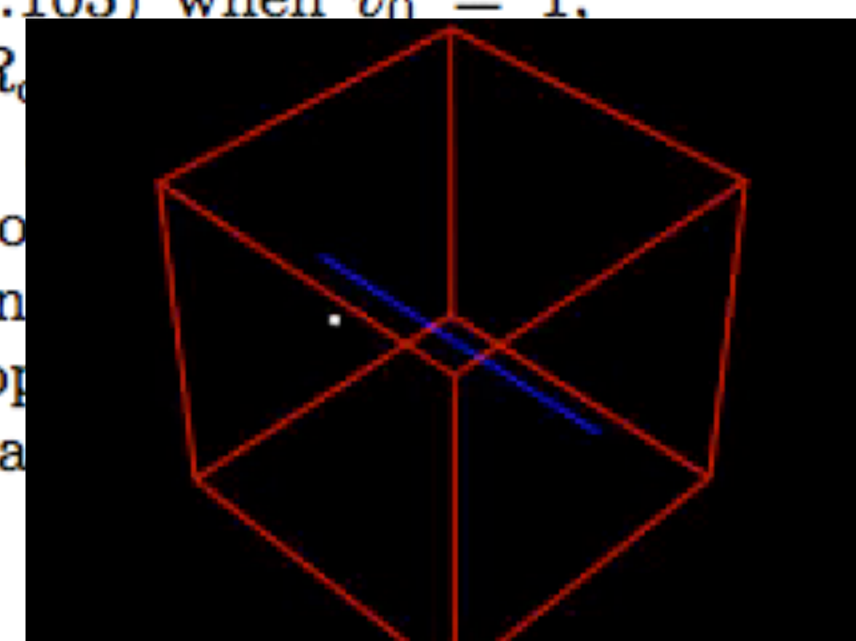

centre-phobic, loop orbit

Angular momentum (z-axis)

$$J = \mathbf{r} \times \mathbf{v} = x v_y - y v_x$$

axi-symmetric potential

$$\Phi_{\mathrm{eff}} = \tfrac{1}{2} v_0^2 \ln\left(R^2 + \frac{z^2}{q^2}\right) + \frac{L_z^2}{2R^2}, \qquad (3.70)$$

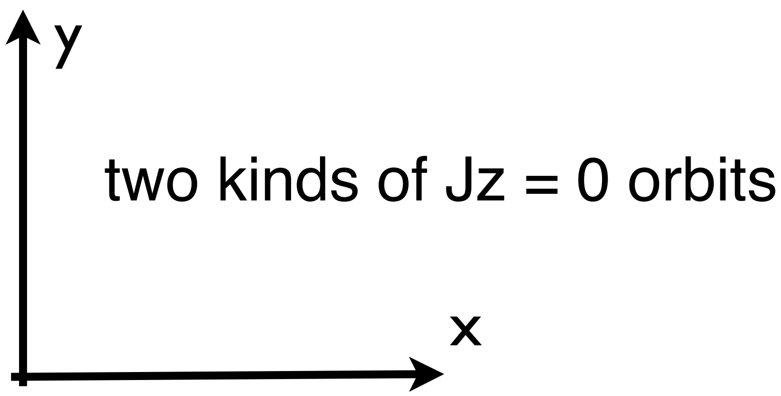

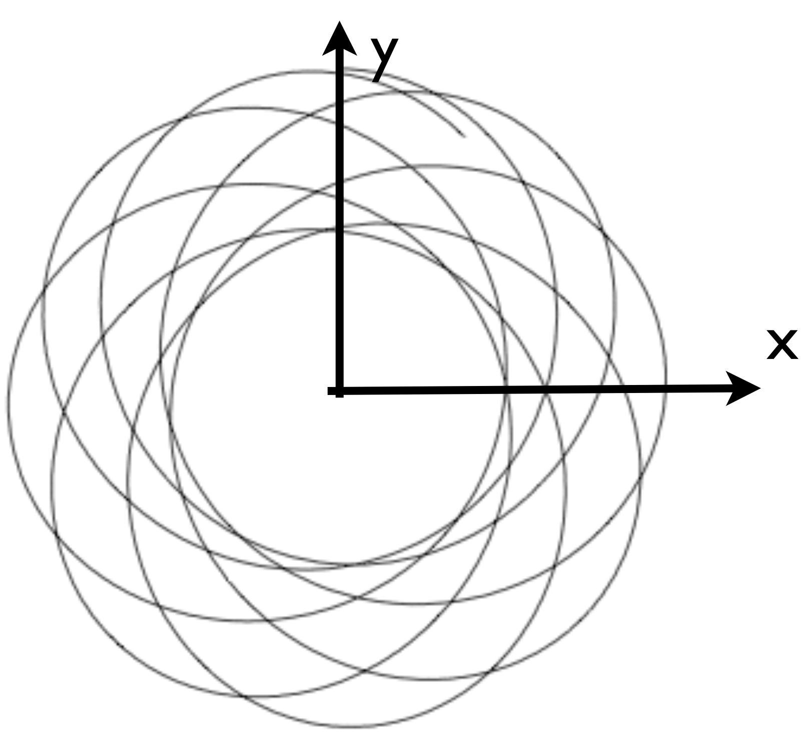

non-axi-symmetric potential (planar)

$$\Phi_{\mathrm{L}}(x, y) = \tfrac{1}{2} v_0^2 \ln\left(R_c^2 + x^2 + \frac{y^2}{q^2}\right) \quad (0 < q \leq 1). \qquad (3.103)$$

J changes sign in boxy orbit (stems from J=0 orbits)

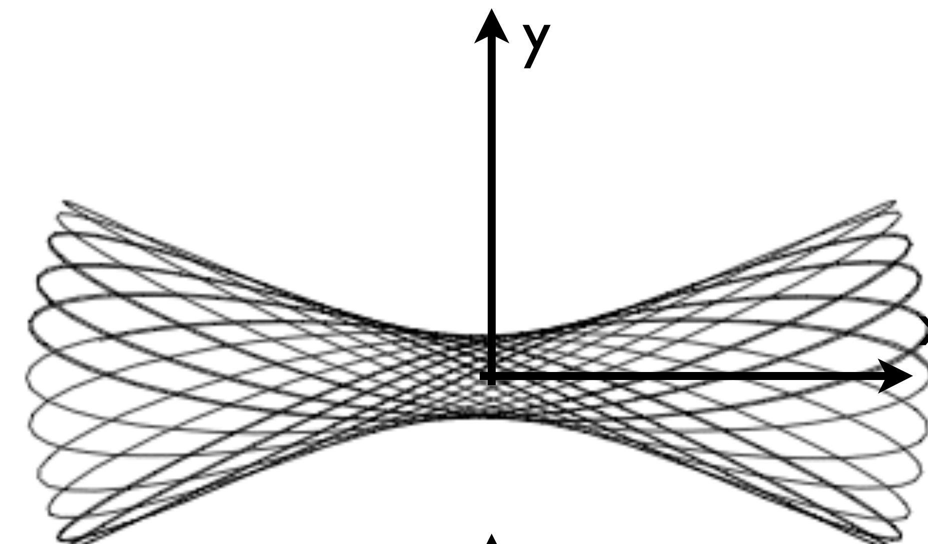

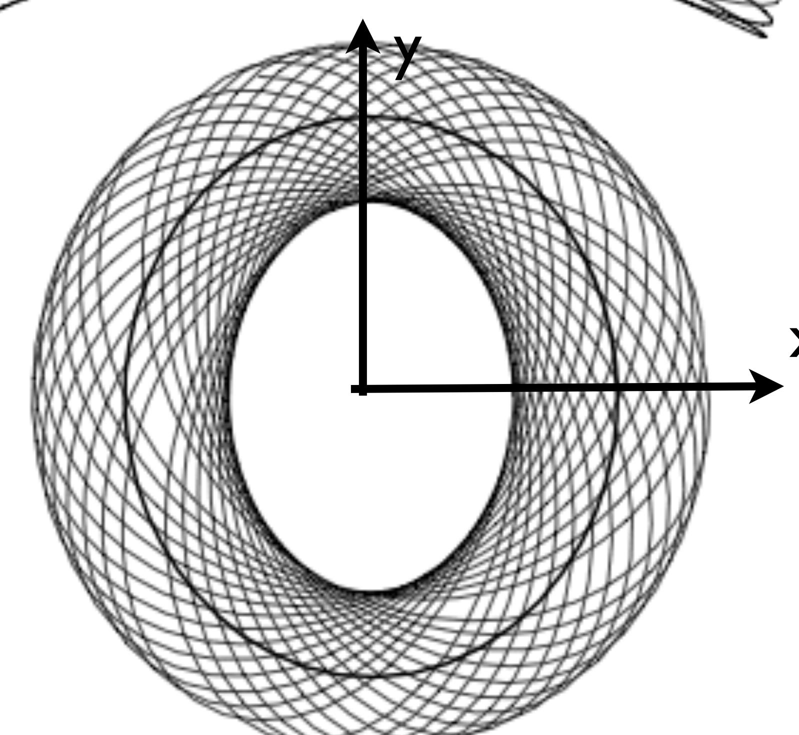

J ~ conserved in loopy orbit (relic of axi-symmetric potential)

transition from loop to box and back: roughly corre. to changing Lz?

J changes sign in boxy orbit (stems from J=0 orbits)

J ~ conserved in loopy orbit (relic of axi-symmetric potential)

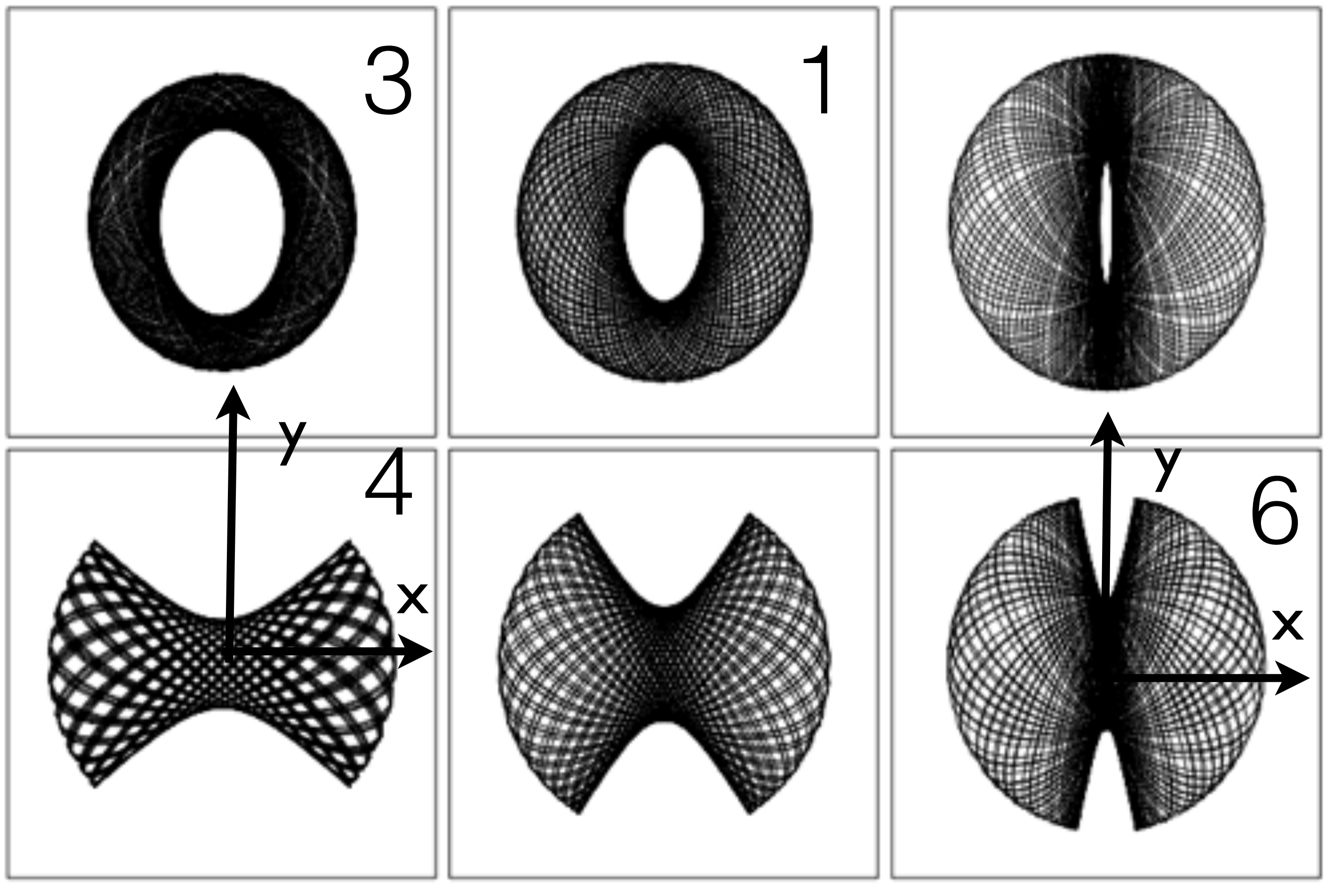

Figure 3.10 A selection of loop (top row) and box (bottom row) orbits in the potential $\Phi_L(q = 0.9, R_c = 0.14)$ at the energy of Figures 3.8 and 3.9.

strobe whenever

$y=0$, $p_y > 0$

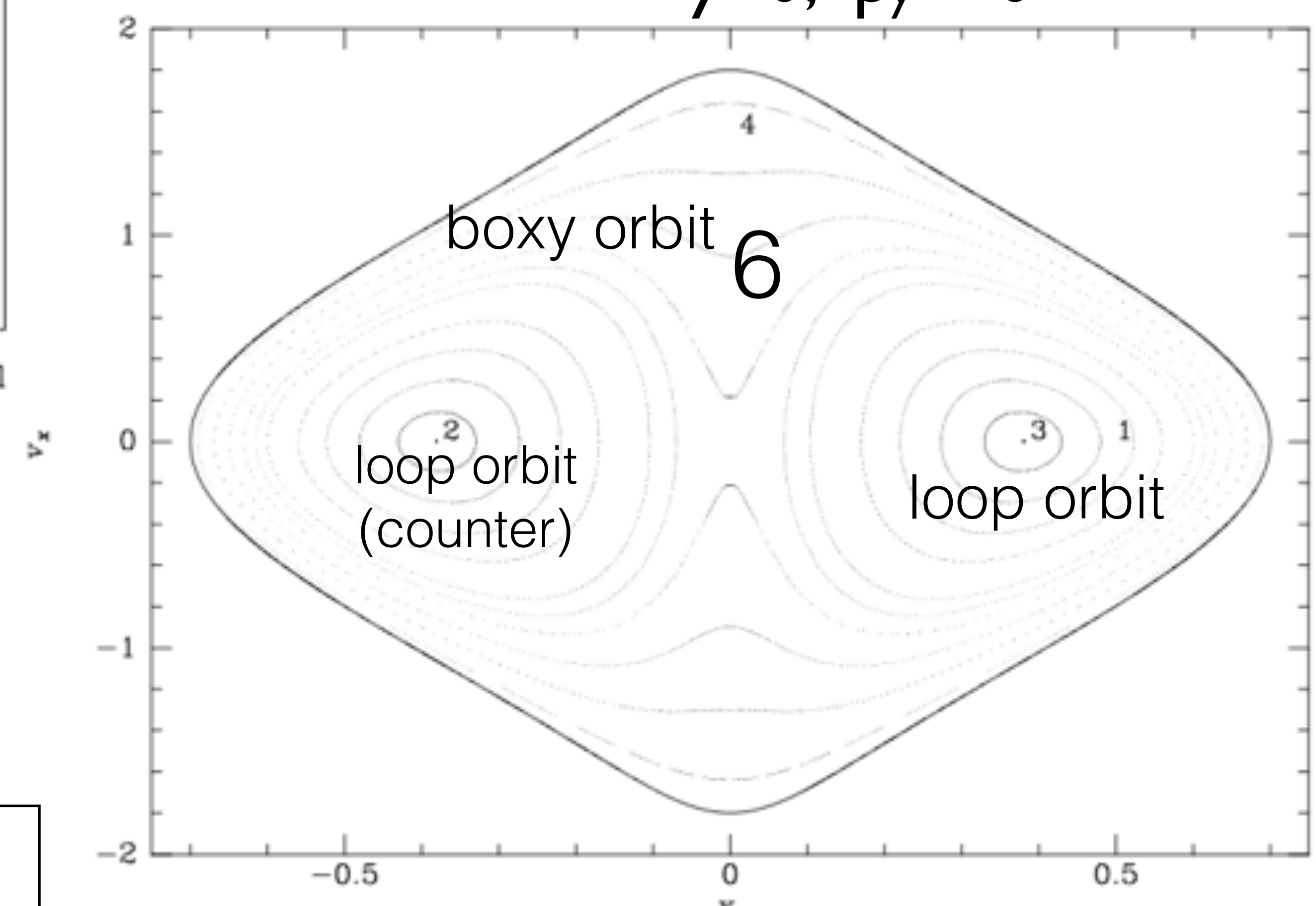

Figure 3.9 The $(x, \dot{x})$ surface of section formed by orbits in Φ_L of the same energy as the orbits depicted in Figure 3.8. The isopotential surface of this energy cuts the long axis at $x = 0.7$. The curves marked 4 and 1 correspond to the box and loop orbits shown in the top and bottom panels of Figure 3.8.

$$\Phi_L(x, y) = \tfrac{1}{2} v_0^2 \ln\left(R_c^2 + x^2 + \frac{y^2}{q^2}\right) \quad (0 < q \leq 1). \tag{3.103}$$

q=0.9

The advance of box

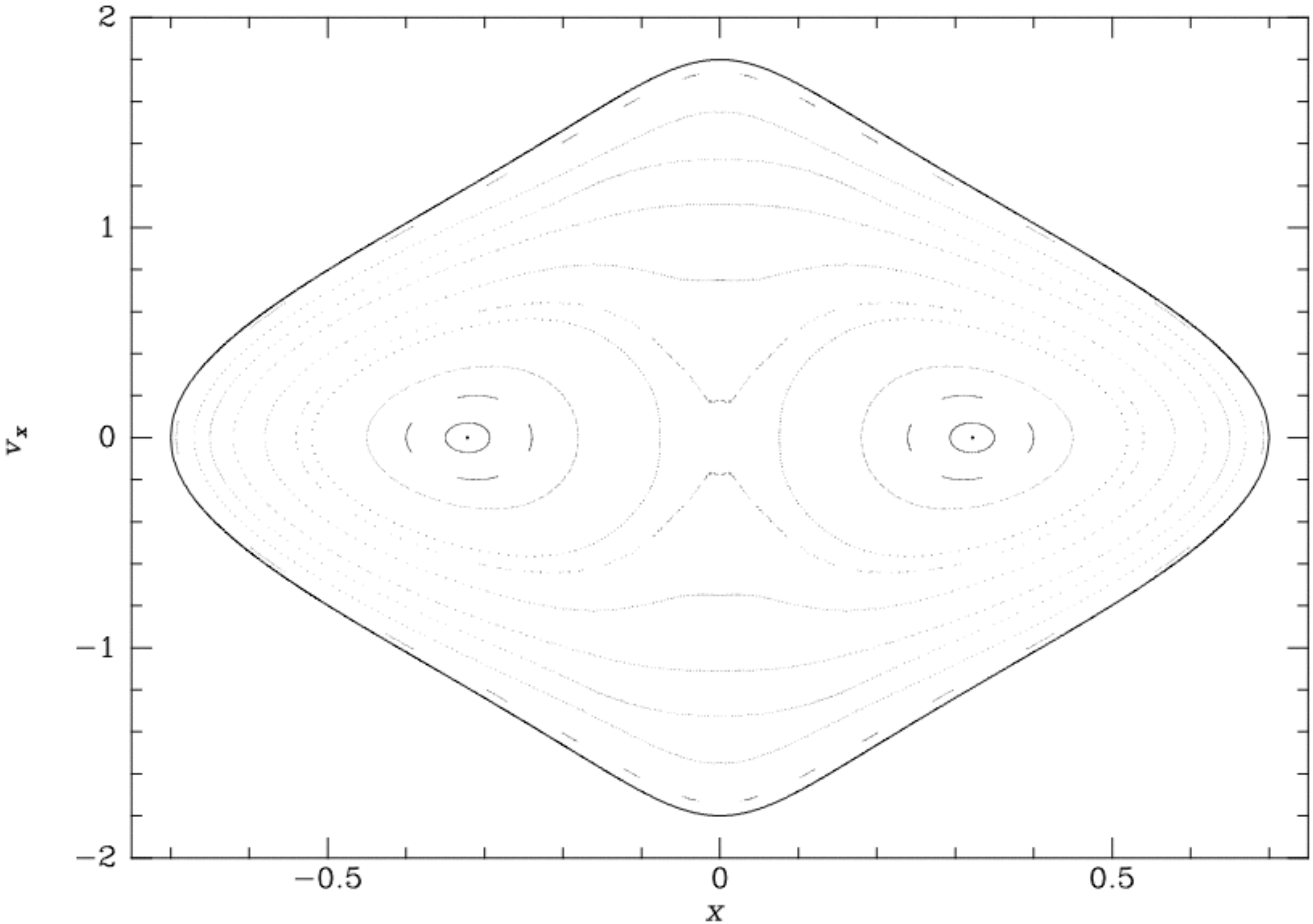

Figure 3.12 When the potential Φ_L is made more strongly barred by diminishing q, the proportion of orbits that are boxes grows at the expense of the loops: the figure shows the same surface of section as Figure 3.9 but for $q = 0.8$ rather than $q = 0.9$.

Possibility of resonant orbits — leading to chaos

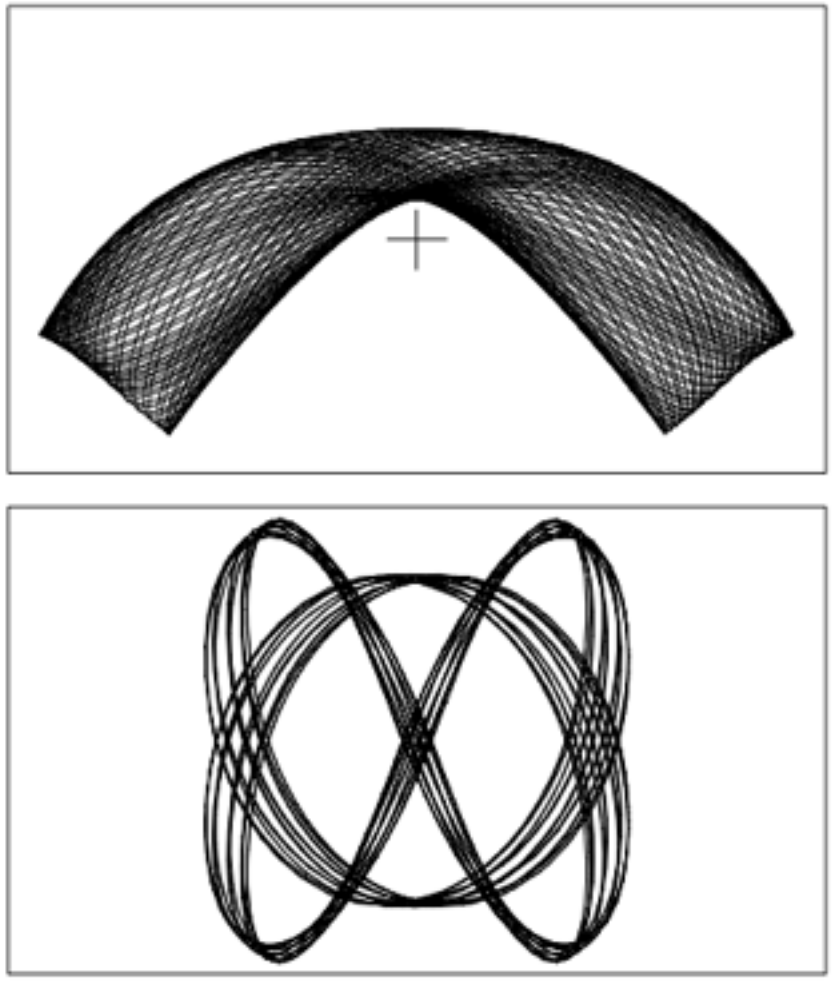

Figure 3.40 The appearance in real space of a banana orbit (top) and a fish orbit (bottom). In the upper panel the cross marks the center of the potential. Resonant box orbits of these types are responsible for the chains of islands in Figure 3.39. The banana orbits generate the outer chain of four islands, and the fish orbits the chain of six islands further in.

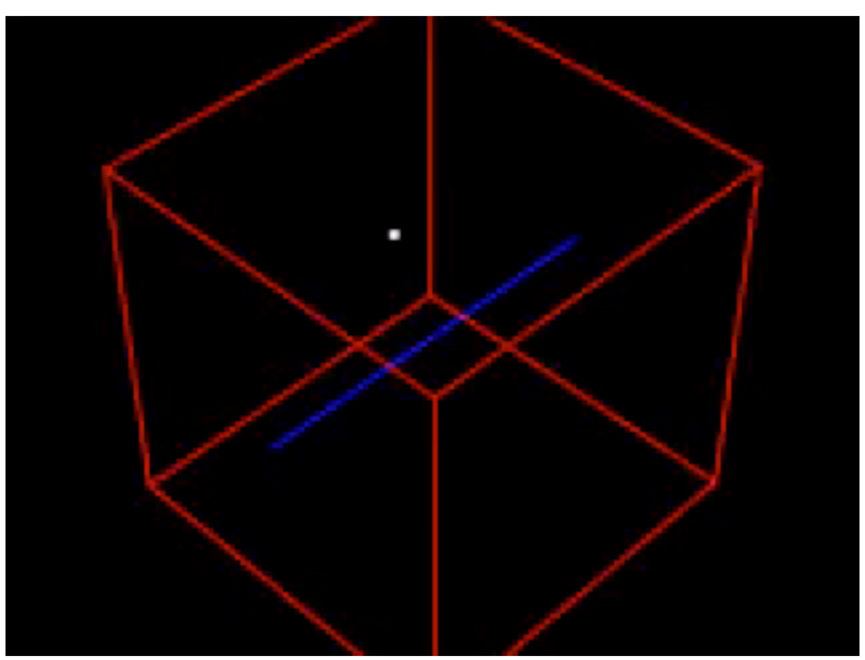

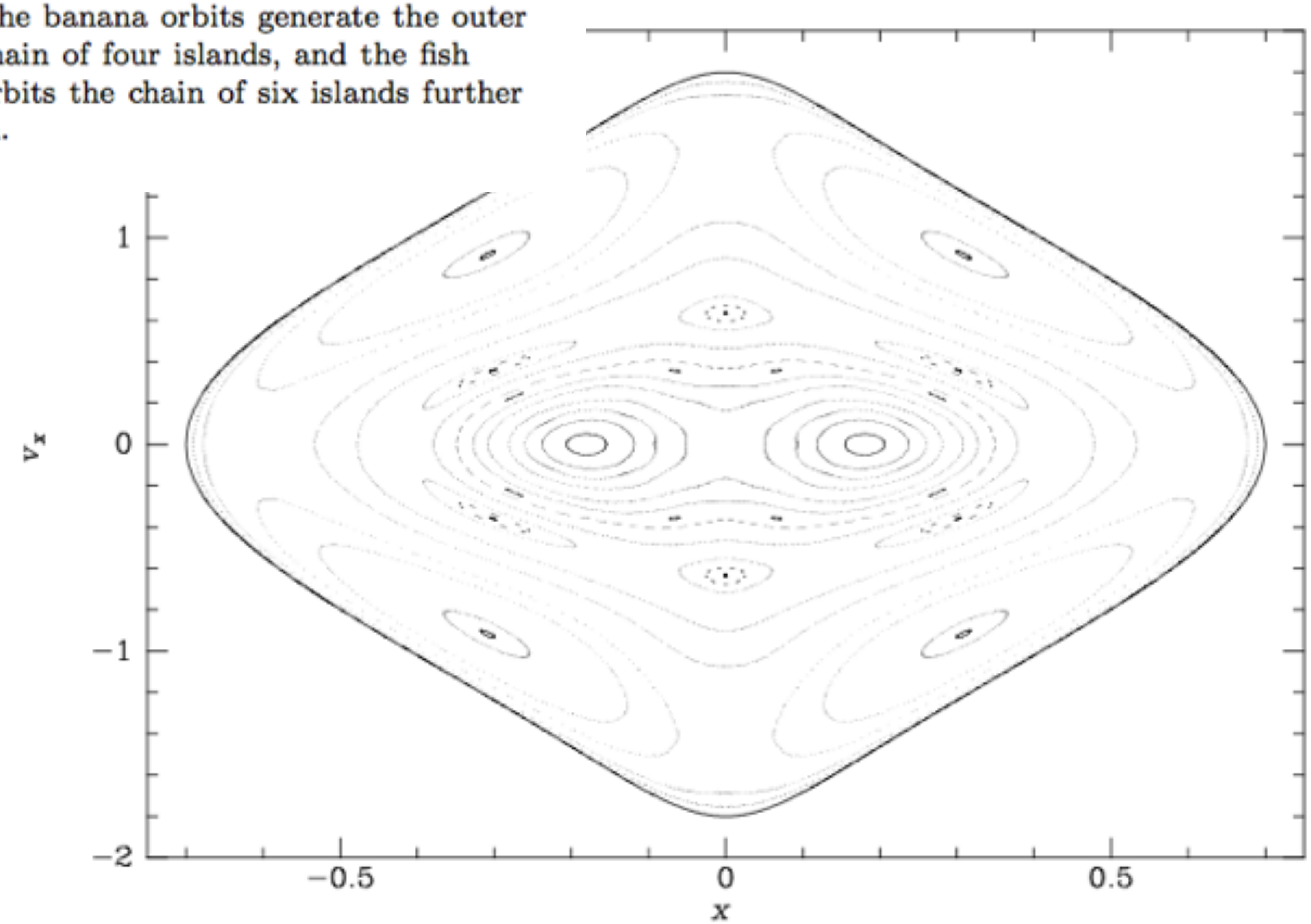

Figure 3.39 A surface of section for motion in Φ_L (eq. 3.103) with $q = 0.6$.

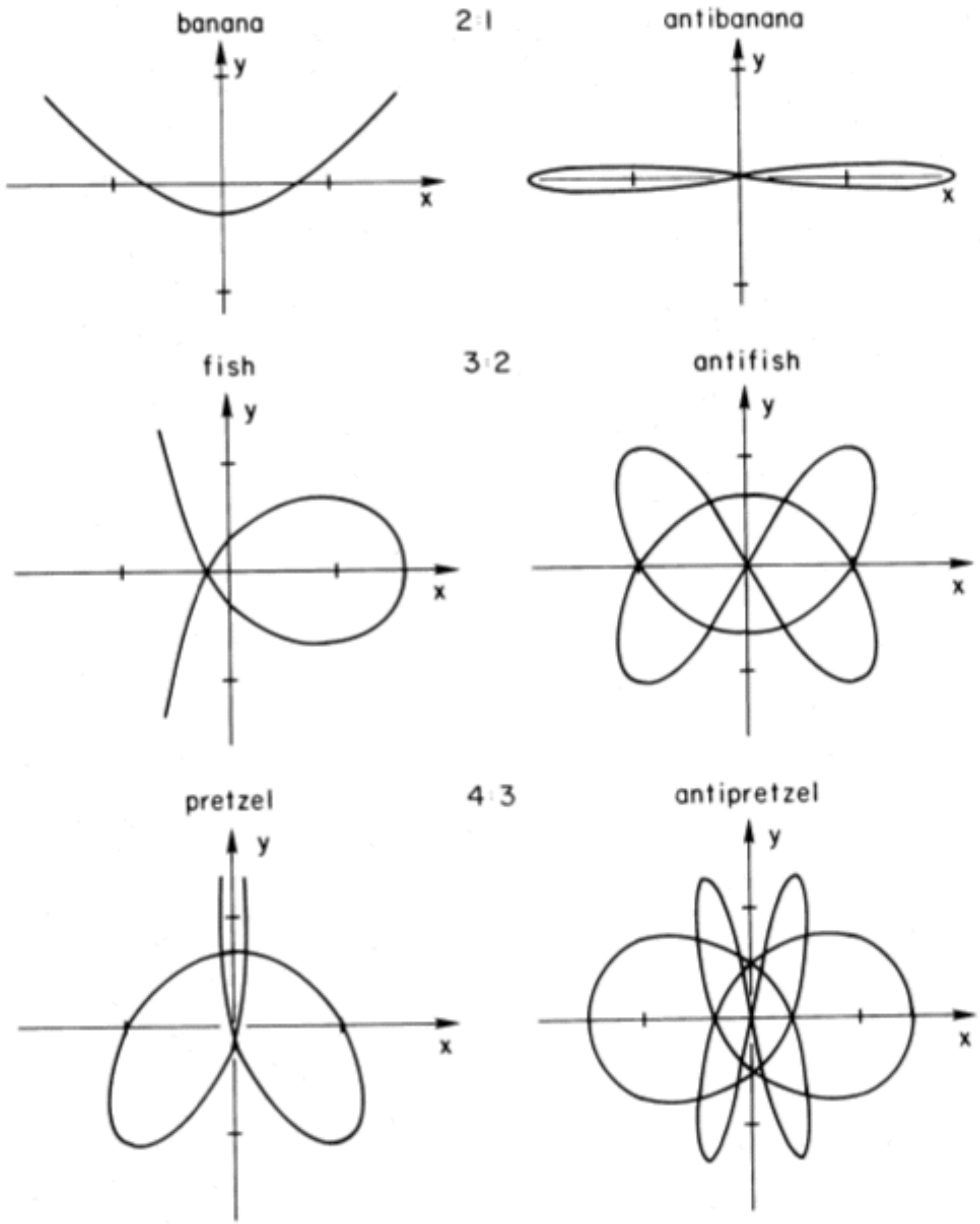

G. 4.—Closed boxlets in the singular logarithmic potential with axis ratio $b = 0.7$. *Left*: centrophobic (stable). *Right*: centrophilic (unstable).

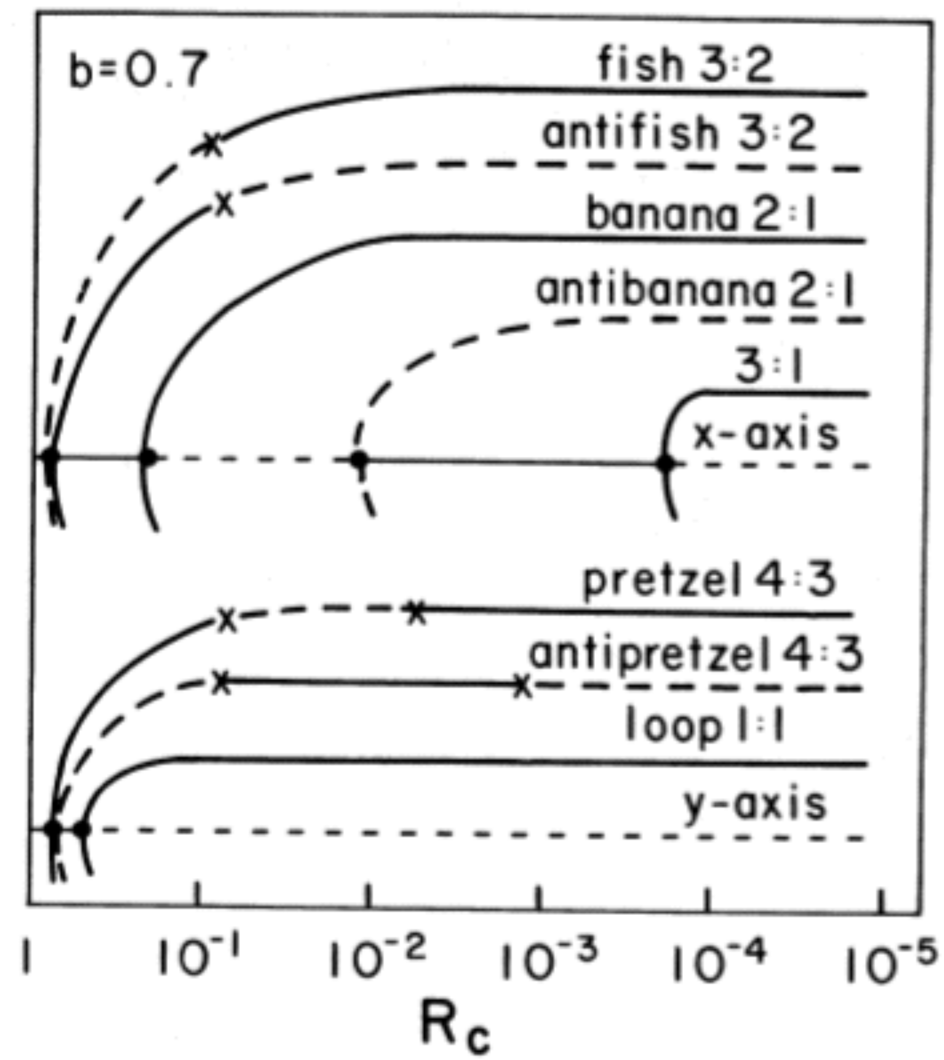

FIG. 5.—Schematic bifurcation diagram for $b = 0.7$. *Solid lines*: stable orbits. *Dashed lines*: unstable orbits. *Dots*: bifurcations of boxlets from axial orbits. *Crosses*: bifurcations of higher resonances from boxlets.

$$\Phi_{\rm L}(x,y) = \tfrac{1}{2}v_0^2 \ln\left(R_{\rm c}^2 + x^2 + \frac{y^2}{q^2}\right) \quad (0 < q \leq 1). \tag{3.103}$$

q=1.0

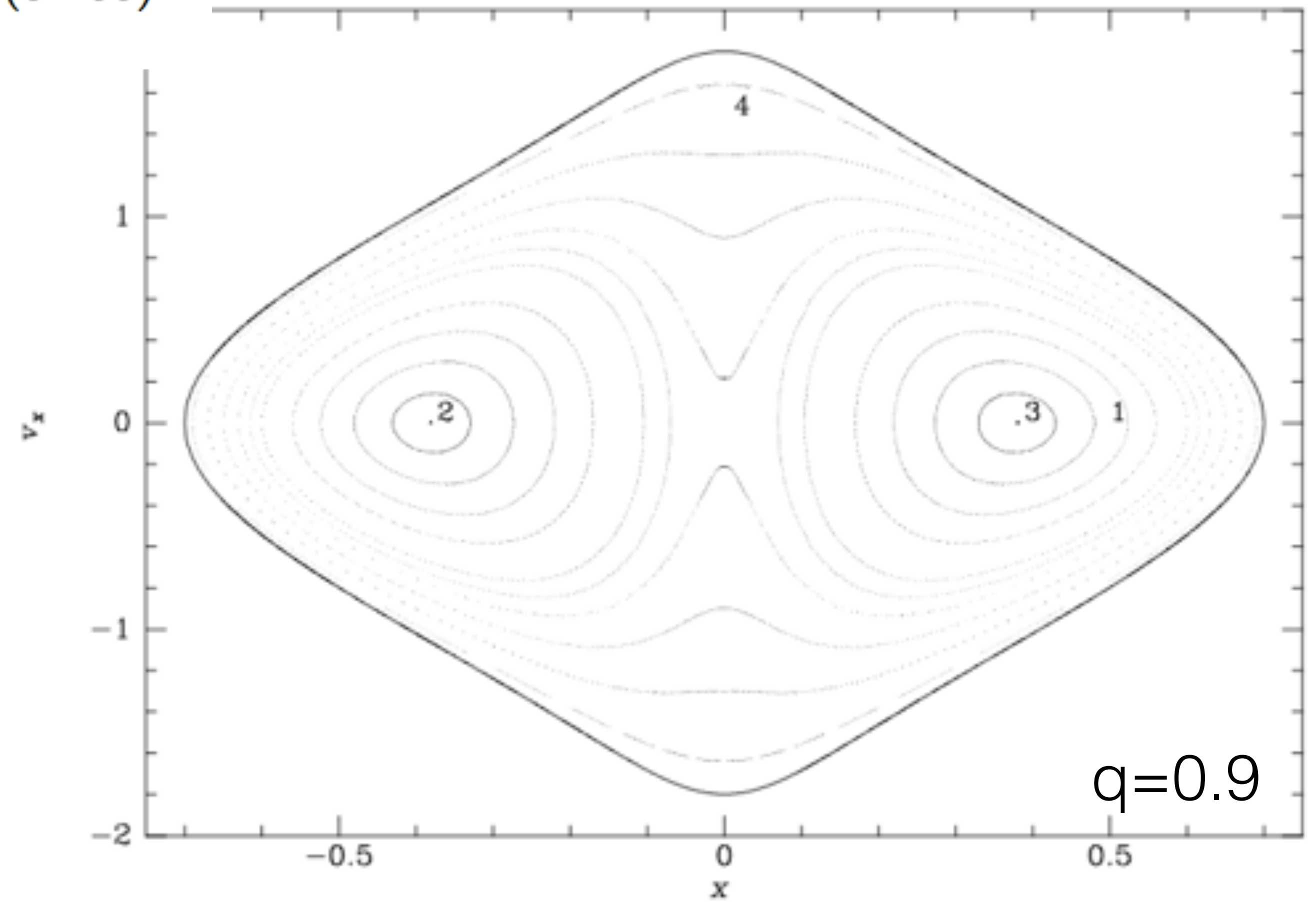

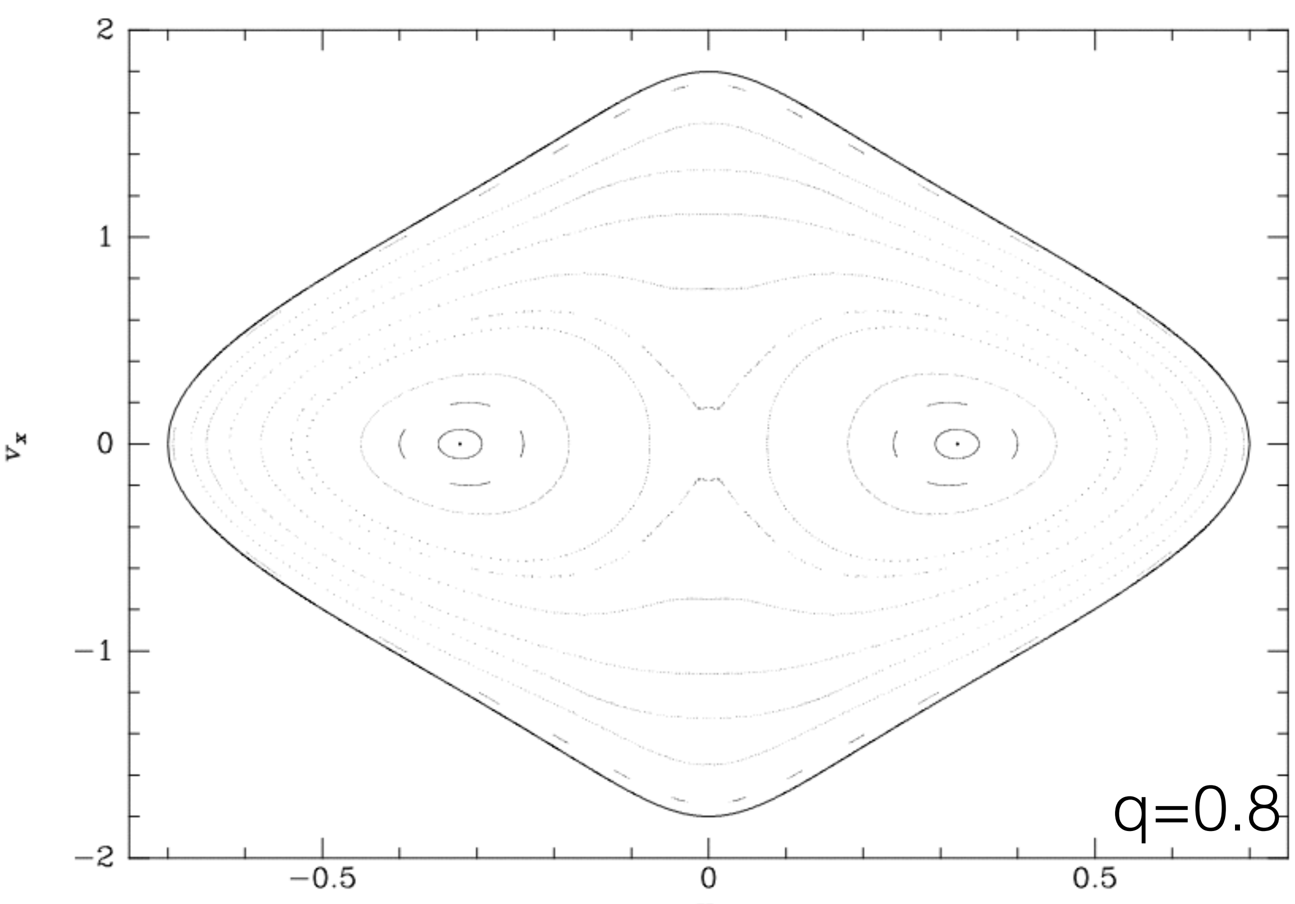

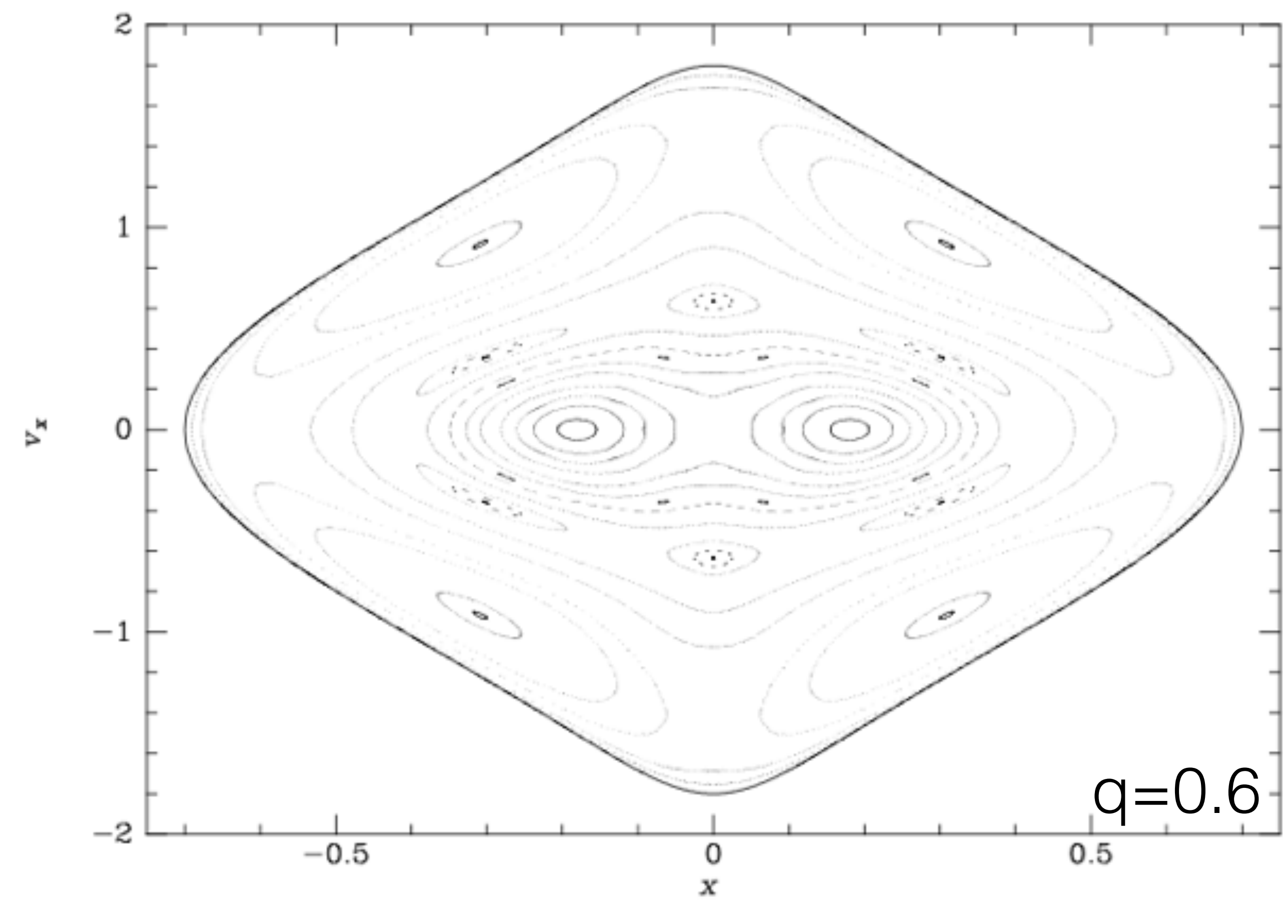

Non-axisymmetric potential

$$\Phi = \Phi(x, y, z)$$

The perfect Ellipsoid (triaxial potential in the Stackel form)

$$\boxed{\rho(\mathbf{x}) = \frac{\rho_0}{(1+m^2)^2} \quad \text{where} \quad m^2 \equiv \frac{x^2 + (y/q_1)^2 + (z/q_2)^2}{a_0^2}. \qquad (3.316)}$$

equation of motion separable in the ellipsoidal coordinates
3 isolating integrals for all orbits

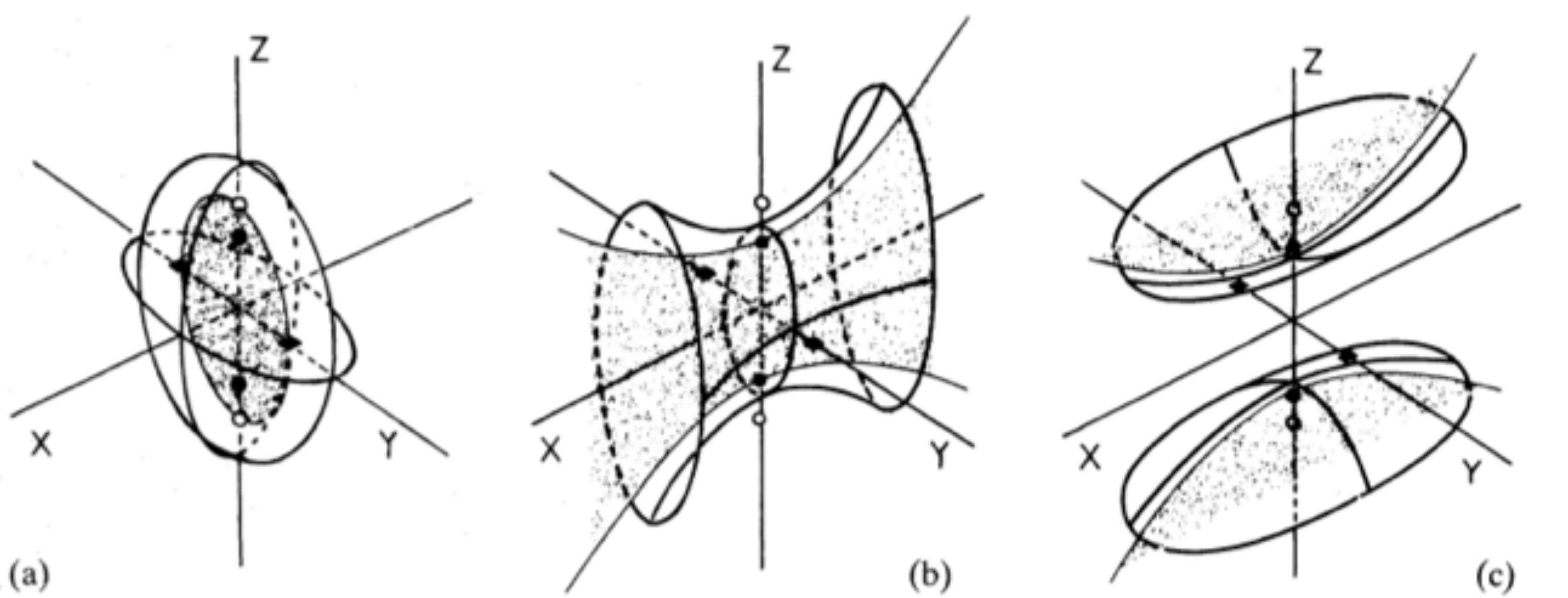

Figure 2. Ellipsoidal coordinates. The three pairs of foci are denoted by the open and filled circles and the filled squares. (a) Surfaces of constant λ are ellipsoids. The degenerate ellipsoid $\lambda = -\alpha$, inside the focal ellipse, is shaded. (b) Surfaces of constant μ are hyperboloids of one sheet. The degenerate hyperboloid $\mu = -\beta$, between the two branches of the focal hyperbola, is shaded. (c) Surfaces of constant ν are hyperboloids of two sheets. The degenerate hyperboloid $\nu = -\beta$ is shaded.

de Zeeuw '85

The perfect ellipsoid supports 4-types of orbit

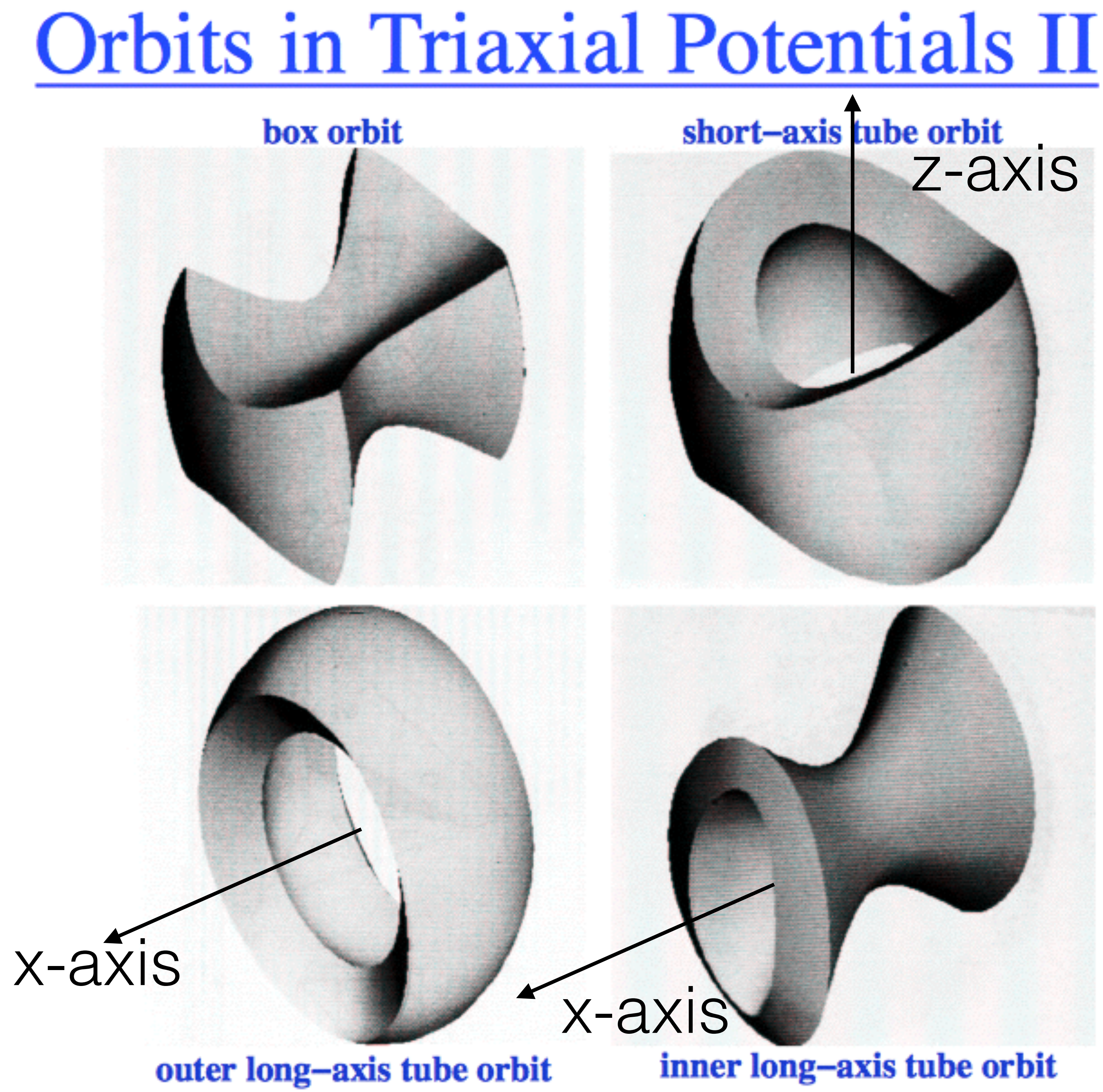

They are the 3-D counterparts of box and loop orbits in 2-D.
Which orbit should gas (closed-orbit) go?

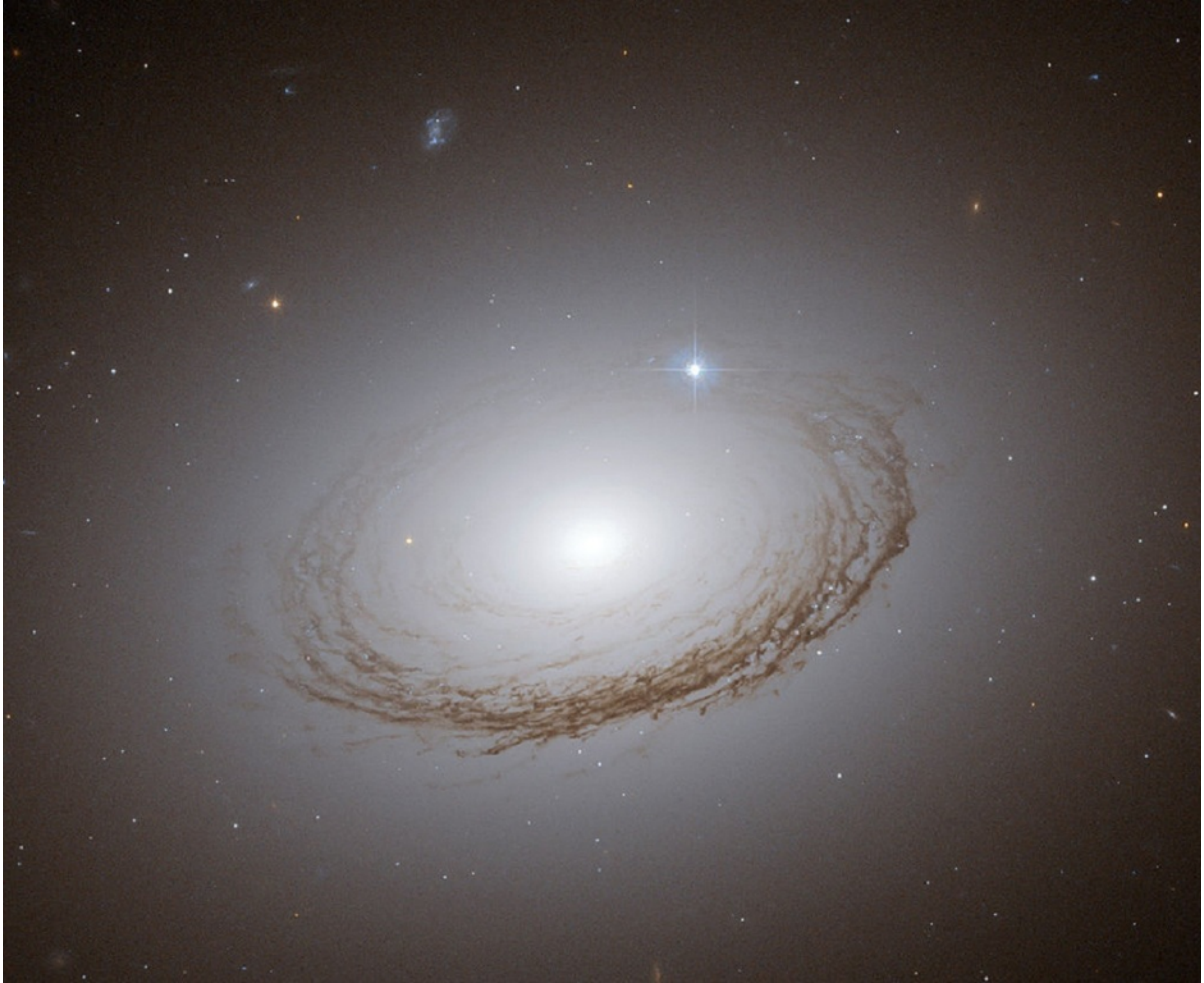

Merritt '93 : Dynamics of Elliptical Galaxies (Science)

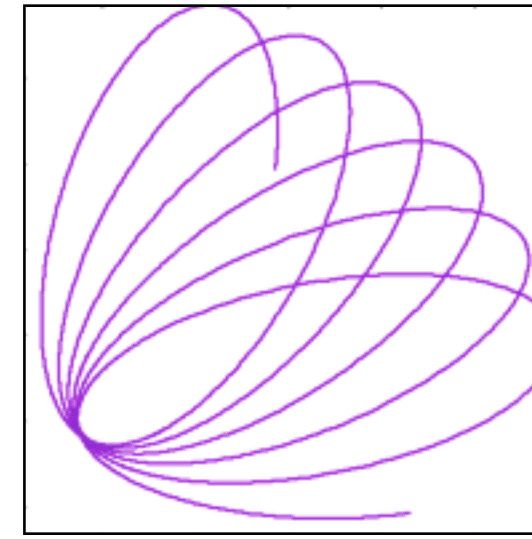

•spherical potential: precessing, planar motion (motion regular)

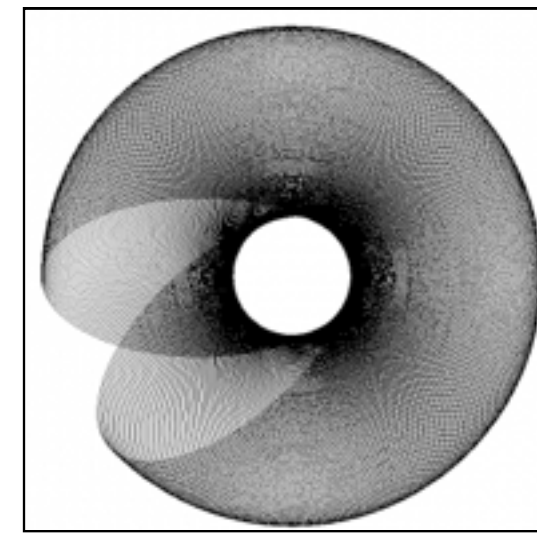

•axisymmetric potential: annular orbit precesses around z-axis, donut-shaped, typically 3 integrals of motion (motion all regular)

•triaxial potential:

when perfect ellipsoid (Stackel potential), regular

when general, often still integrals of motion

4 family of orbits

--box: centrophilic, dominating elliptical galaxies, but easily perturbed by central density/BH

--loop: centrophobic, 3-groups, have net J.

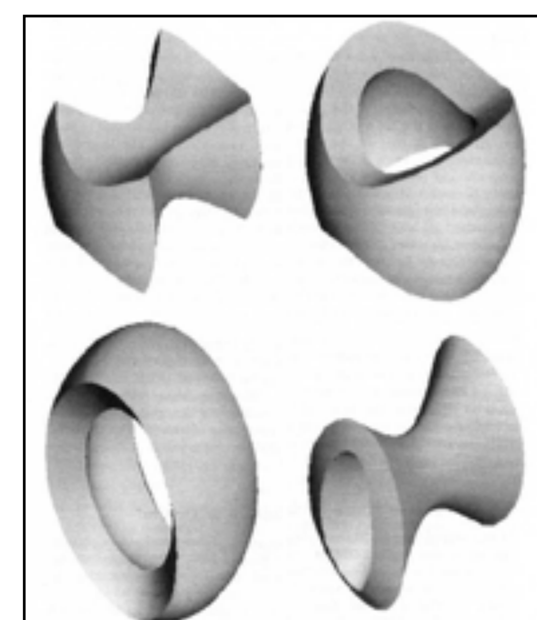

orbits in perfect ellipsoids have 3 integrals of motion:

I_1, I_2, I_3

distribution function: $f(I_1, I_2, I_3)$

use spectral data to extract f

— **the Schwarzschild method**

Schwarzschild Modelling

Why model galaxies?

adapted from a lecture by
Dr. Anne-Marie Weijmans

- We want to understand how galaxies formed and evolved
  - star formation history
  - merger and accretion events
- Look in detail at nearby galaxies, unravel their formation history (fossil record)
  - 'galactic archeology'
- Use dynamical models to study their dynamical structure

Extracting kinematics from spectra

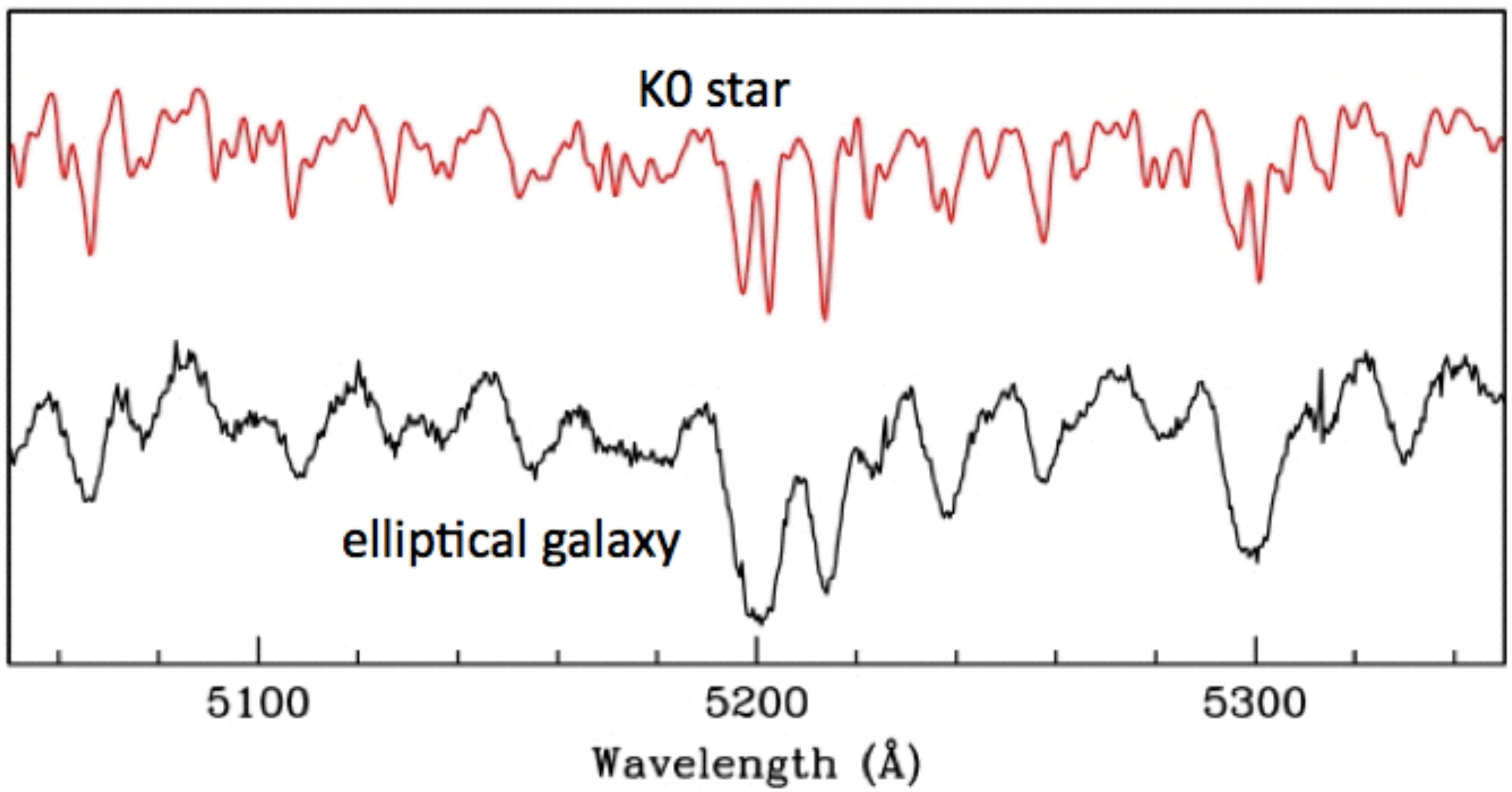

- Galaxy spectrum is composed of stellar spectra
- Stellar spectra convolved with LOSVD
  - LOSVD = line-of-sight velocity distribution
  - stellar reference spectrum is shifted and broadened

mean velocity velocity dispersion

Line-Of-Sight Velocity Distribution

all these are mapped on the sky plane;
so a superposition of depth

- Assume LOSVD is Gaussian
  - measure mean and standard deviation
- But allow for deviations from true Gaussian
  - skewness $\xi_3 \rightarrow$ asymmetrical deviations
  - kurtosis $\xi_4 \rightarrow$ symmetrical deviations
  - deviations caused by orbital structure

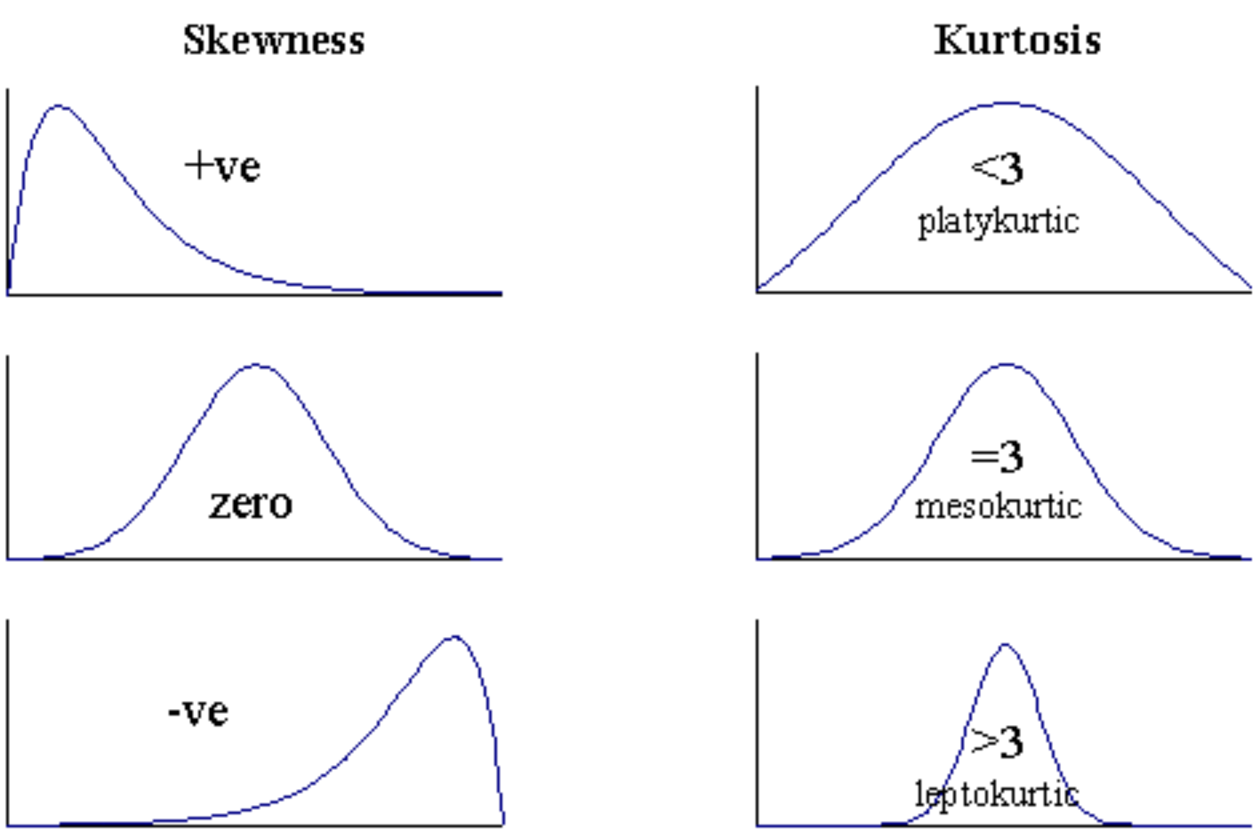

$$\mathrm{E}[X] = \mu.$$

$$\sigma = \sqrt{\mathrm{E}[(X-\mu)^2]}$$

$$\gamma_1 = \mathrm{E}\left[\left(\frac{X-\mu}{\sigma}\right)^3\right] = \frac{\mu_3}{\sigma^3}$$

$$\beta_2 = \frac{\mathrm{E}[(X-\mu)^4]}{(\mathrm{E}[(X-\mu)^2])^2} = \frac{\mu_4}{\sigma^4}$$

An example of Skewness

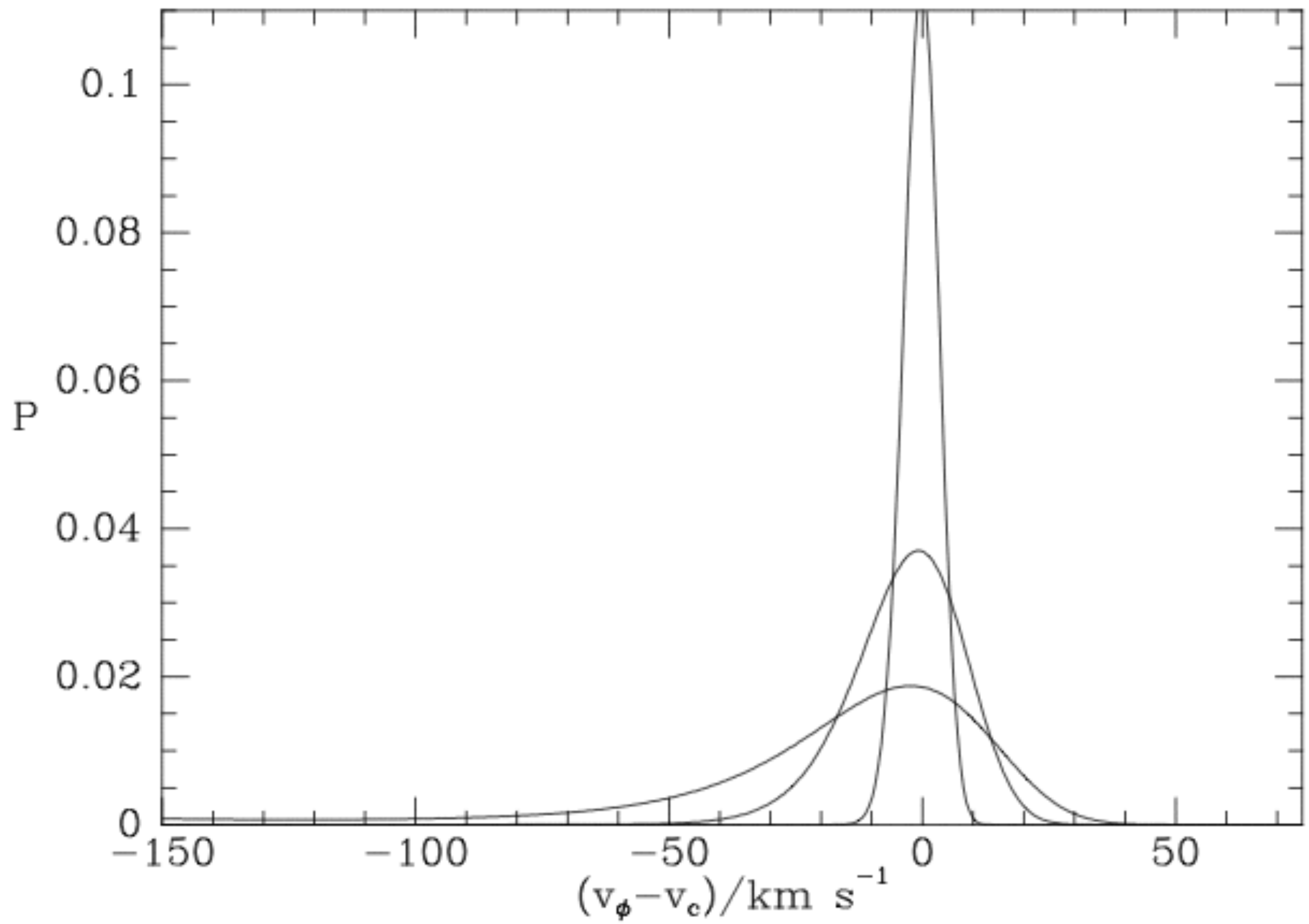

Figure 4.15 Three distributions of azimuthal velocities $\widetilde{v}_\phi$ predicted for stellar populations in the solar neighborhood by the DF (4.156). The circular speed has been assumed to be $v_0 = 220\,\mathrm{km\,s^{-1}}$ at all radii, $\sigma_R(L_z)$ and $\sigma_z(L_z)$ are taken to be proportional to $\exp[-L_z/(2v_0R_\mathrm{d})]$, while $\Sigma = \Sigma_0 \exp(-R/R_\mathrm{d})$, with $R_0/R_\mathrm{d} = 3.2$ (Table 1.2). The values of $\overline{v_R^2}^{1/2}$ for the three populations are 5, 15 and $30\,\mathrm{km\,s^{-1}}$, the largest value producing the widest spread in $\widetilde{v}_\phi$.

real data

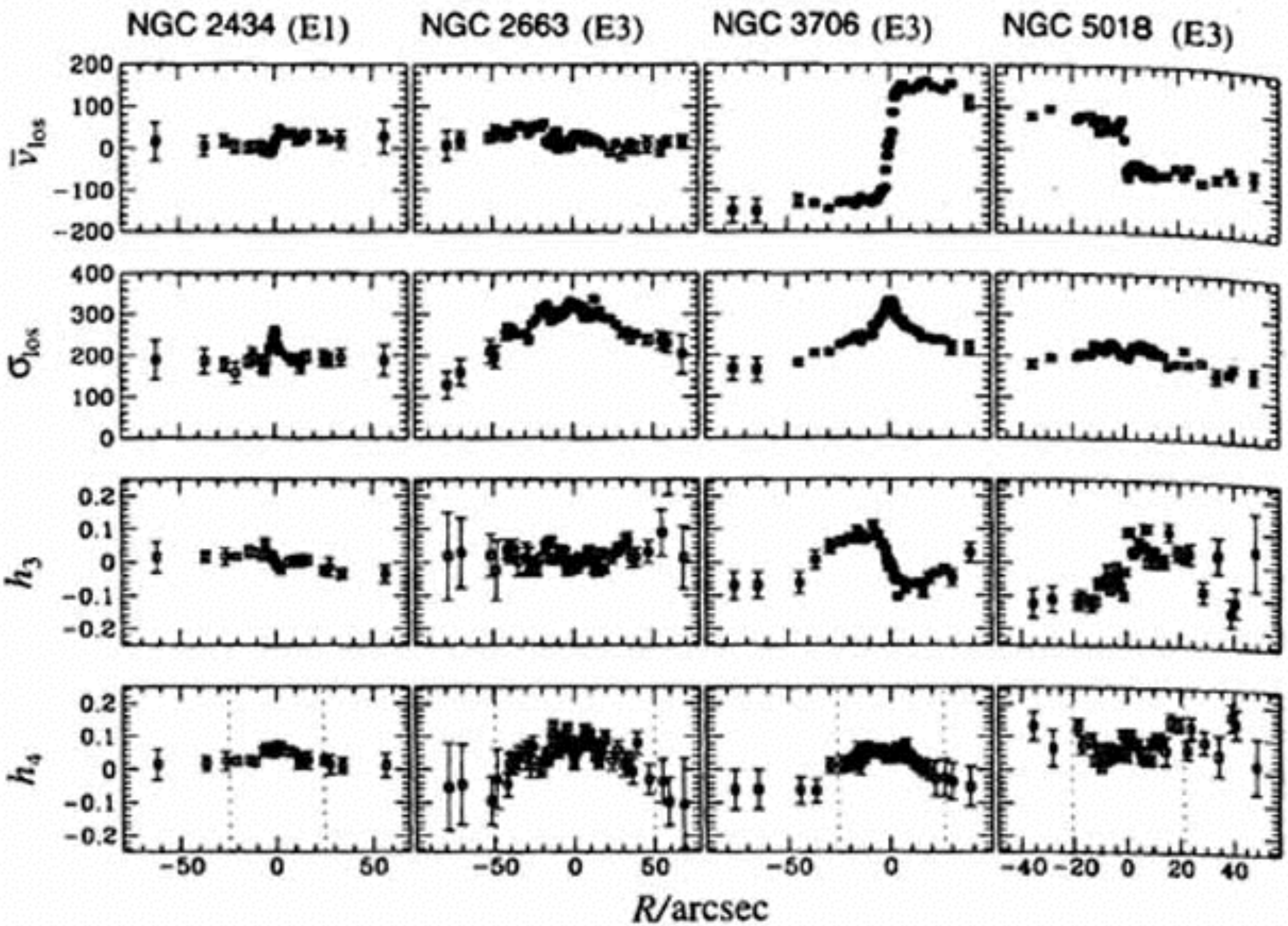

Figure 11.6 The large-scale major-axis kinematics for a sample of four giant elliptical galaxies. The LOSVDs of these systems have been parameterized using the truncated Gauss-Hermite expansion (§11.1.2). The dotted lines indicate the effective radius, R_e, for each galaxy. The Hubble classification (shown in parentheses) is based on the galaxy's average ellipticity outside $R_e/2$. [After Carollo *et al.* (1995)]

Dynamical models

- Jeans models (see previous lectures)
  - only require V and σ
  - analytical solutions (fast!)
  - assumptions: axisymmetry and constant anisotropy
- N-body models (see John Dubinski's lecture)
  - numerical computation
  - no assumptions on shape or orbital structure
  - possible to evolve model (test for stability)
- Schwarzschild models (this lecture)
  - orbital superposition method (faster than N-body)
  - no assumptions on shape or orbital structure

Schwarzschild modeling

Schwarzschild (1979)

- Choose gravitational potential for galaxy
- Calculate orbits in that specific potential
- Find orbit combination that best reproduces observables
  - use non-lineair least square fitting
  - regularize to have smooth distribution function (DF)
  - fit to observed surface brightness and kinematics
- Run variety of models with different potentials, find the one that fits best
  - fit for viewing angles, mass-to-light ratio, black hole mass, etc.

also orbits need to be self-consistent with density distribution

Orbital super-position method

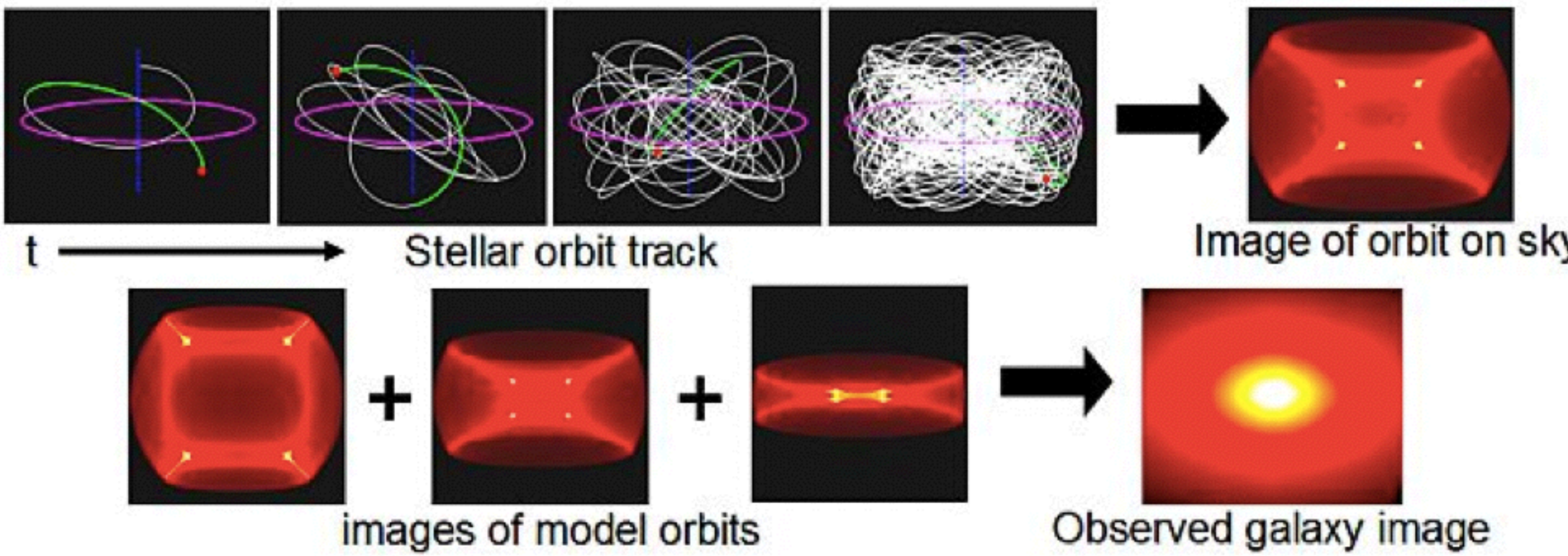

Cappellari et al. 2004

Why Schwarzschild models?

- Schwarzschild models are very general
  - no assumptions on shape, anisotropy etc.
- Resulting models show structure of galaxy
  - mass components, such as hidden discs
  - shape and orbital structure
- Schwarzschild models are relatively fast
  - instead of millions of particles, follow few thousand orbits
- But: Schwarzschild models cannot deal with evolving potentials (bars, spiral arms)
  - mostly used for early-type galaxies

How to recognize a (hidden) disc

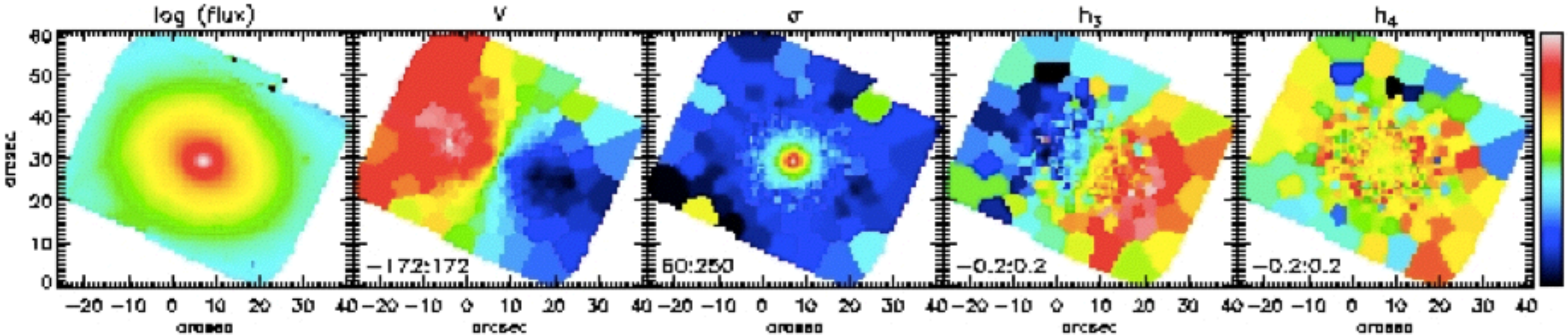

Lam, Meyer & Zhao

- Velocity field shows regular rotation
- h_3 anti-correlates with V
  - broad non-rotating distribution
  - rapidly rotating narrow distribution

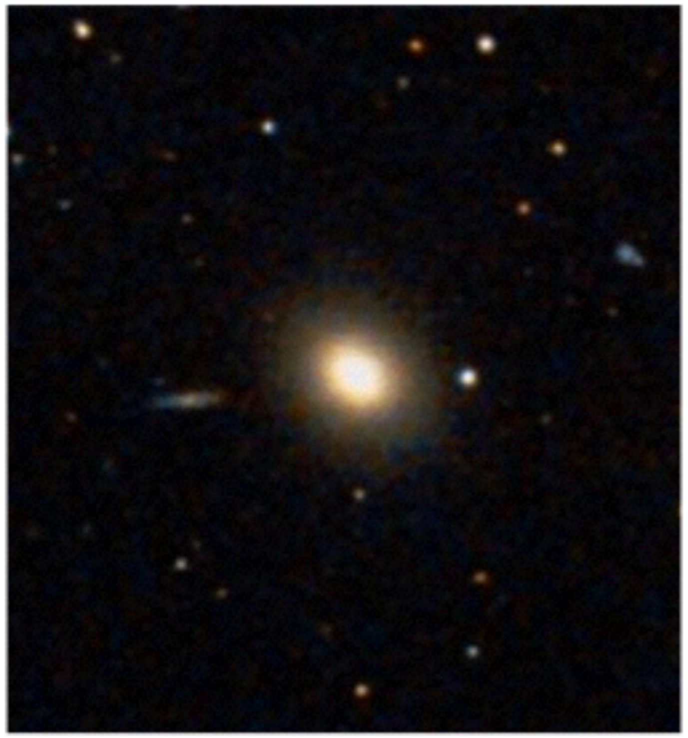

NGC 2592 (SDSS)

Integral Field Spectrograph (IFU)

Integral-field Spectrography

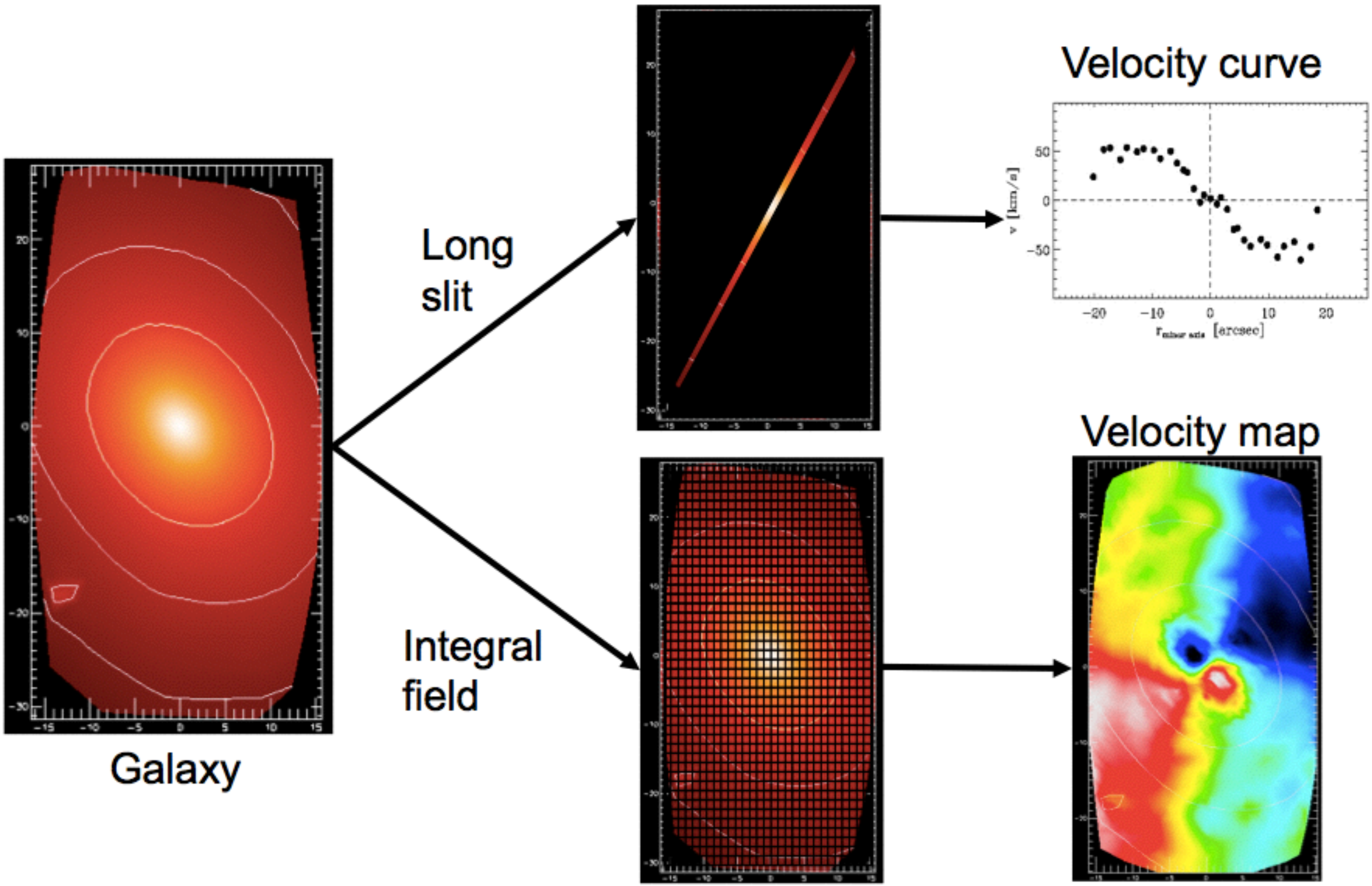

How to recognize triaxiality

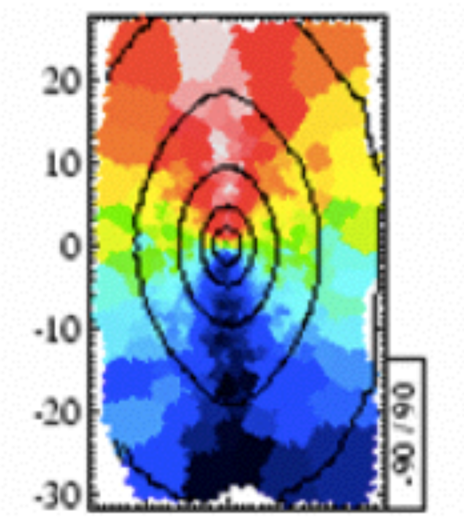

← aligned

misaligned →

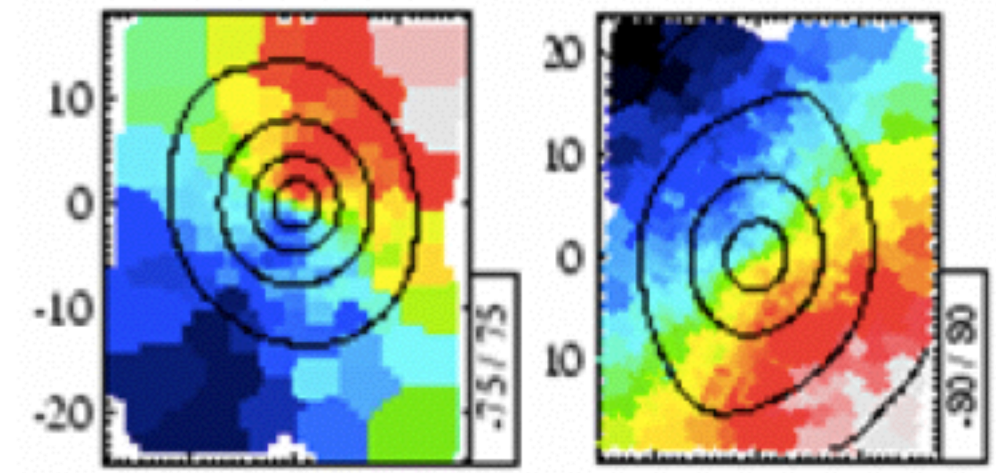

- Axisymmetric galaxy → only short axis orbits
  - rotation axis always aligned with minor axis
- Triaxial galaxy → both short and long axis orbits
  - rotation axis in plane of short and long axis
  - projection of short axis depends on viewing angle
  - rotation axis misaligned from minor axis

Data

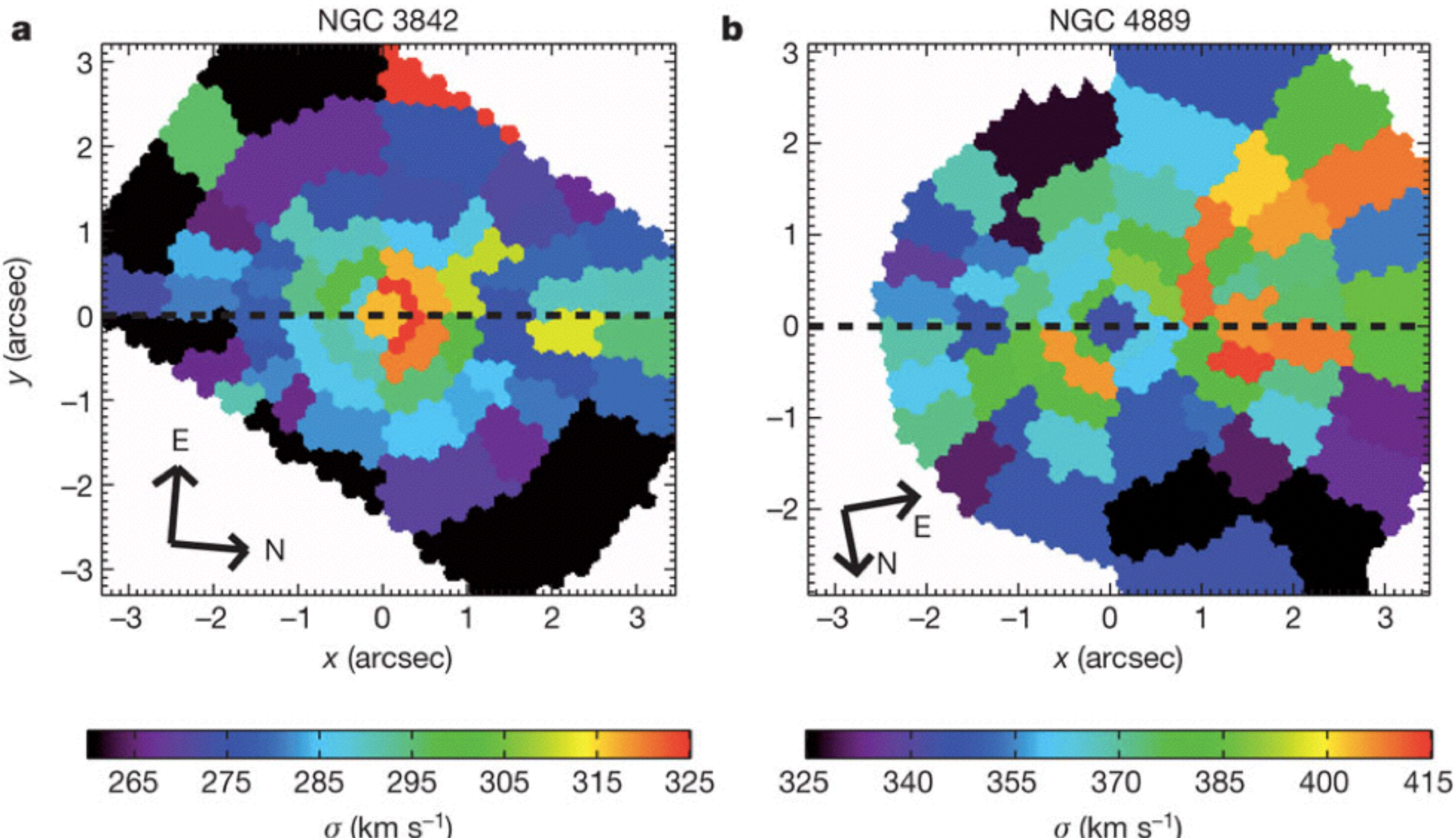

Can we see a black hole in these dispersion maps?

“A Dearth of Dark Matter in Ordinary Elliptical Galaxies”

vs

“Lost and Found Dark Matter in Elliptical Galaxies”

No dark matter in ellipticals?

Romanowsky et al. (2003)

- Obtained PNe measurements for three intermediate luminosity ellipticals
- Data show declining dispersion profiles
- Models required not much (if any) dark matter to fit the observations

http://adsabs.harvard.edu/abs/2003Sci...301.1696R

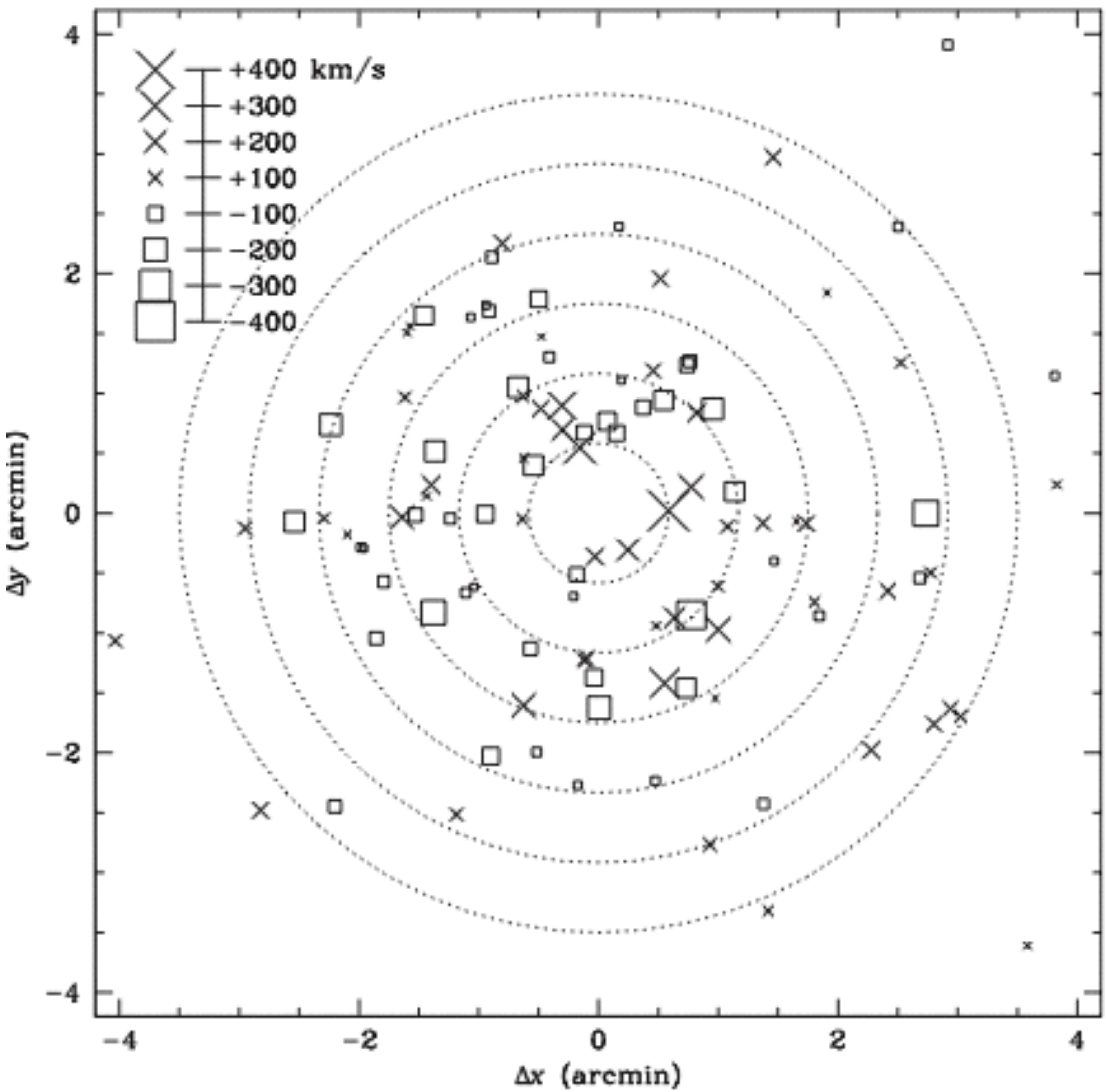

Fig. 1. NGC 3379 with 109 PN line-of-sight velocities relative to the systemic velocity, as measured with the 4.2-m William Herschel Telescope and the PN.S instrument. The symbol sizes are proportional to the velocity magnitudes. A modified version of the data is shown in fig. S1. Similar data were obtained for NGC 821 and NGC 4494 (figs. S2 and S3). Crosses indicate receding velocities; boxes, approaching velocities; dotted circles, isophotes in increments of R_{eff}.

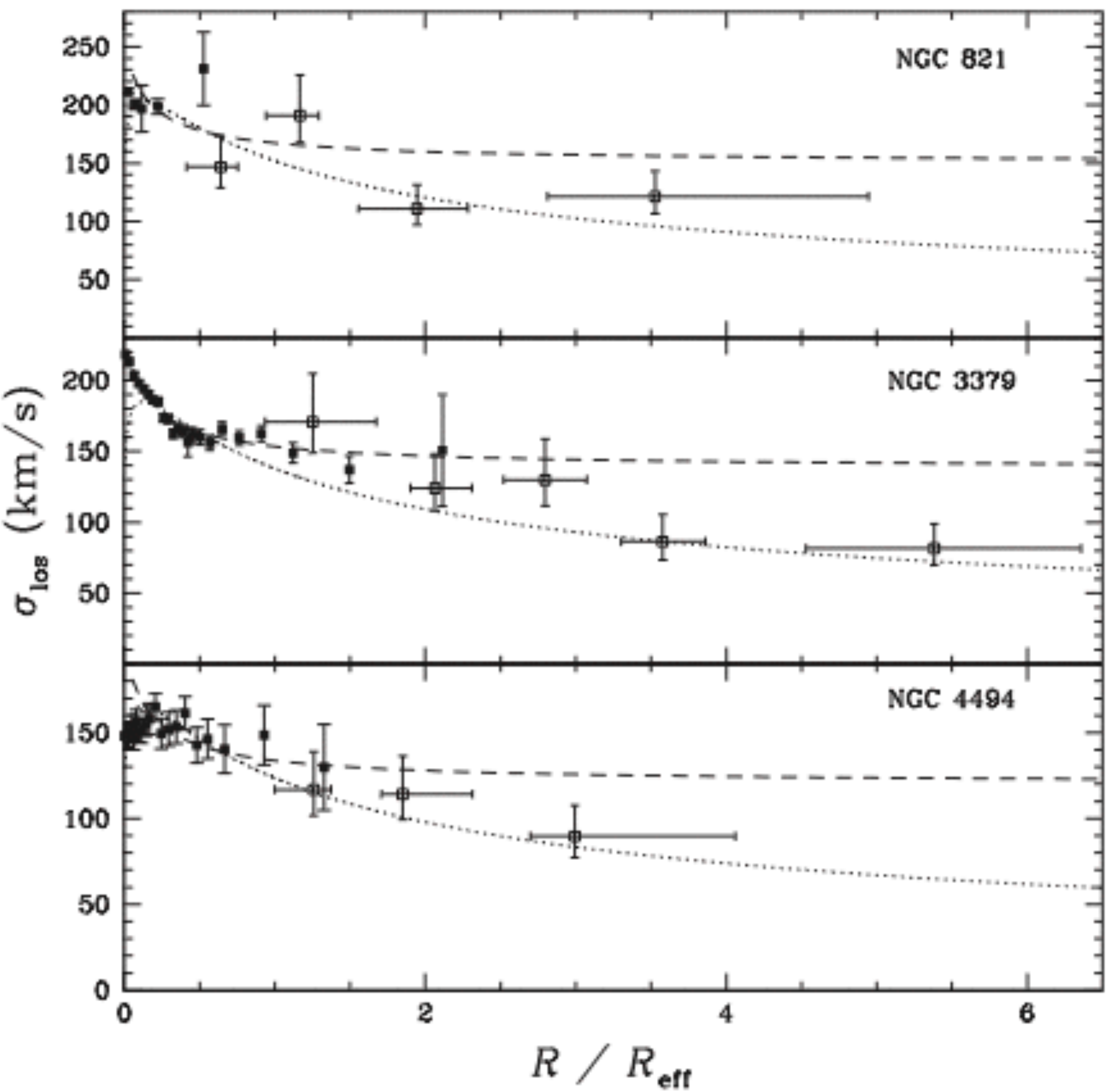

Fig. 2. Line-of-sight velocity dispersion profiles for three elliptical galaxies, as a function of projected radius in units of R_{eff}. Open points show planetary nebula data (from the PN.S); solid points show diffuse stellar data (*12–14*). The vertical error bars show 1σ uncertainties in the dispersion, and the horizontal error bars show the radial range covered by 68% of the points in each bin. Predictions of simple isotropic models are also shown for comparison: a singular isothermal halo (dashed lines) and a constant mass-to-light–ratio galaxy (dotted lines).

Lost & found dark matter in elliptical galaxies

A. Dekel[1,2,3], F. Stoehr[2], G.A. Mamon[2], T.J. Cox[4], G.S. Novak[5], & J.R. Primack[3]

- Constructed numerical simulations of disc-galaxy mergers to form ellipticals
- Mergers result in elongated stellar orbits

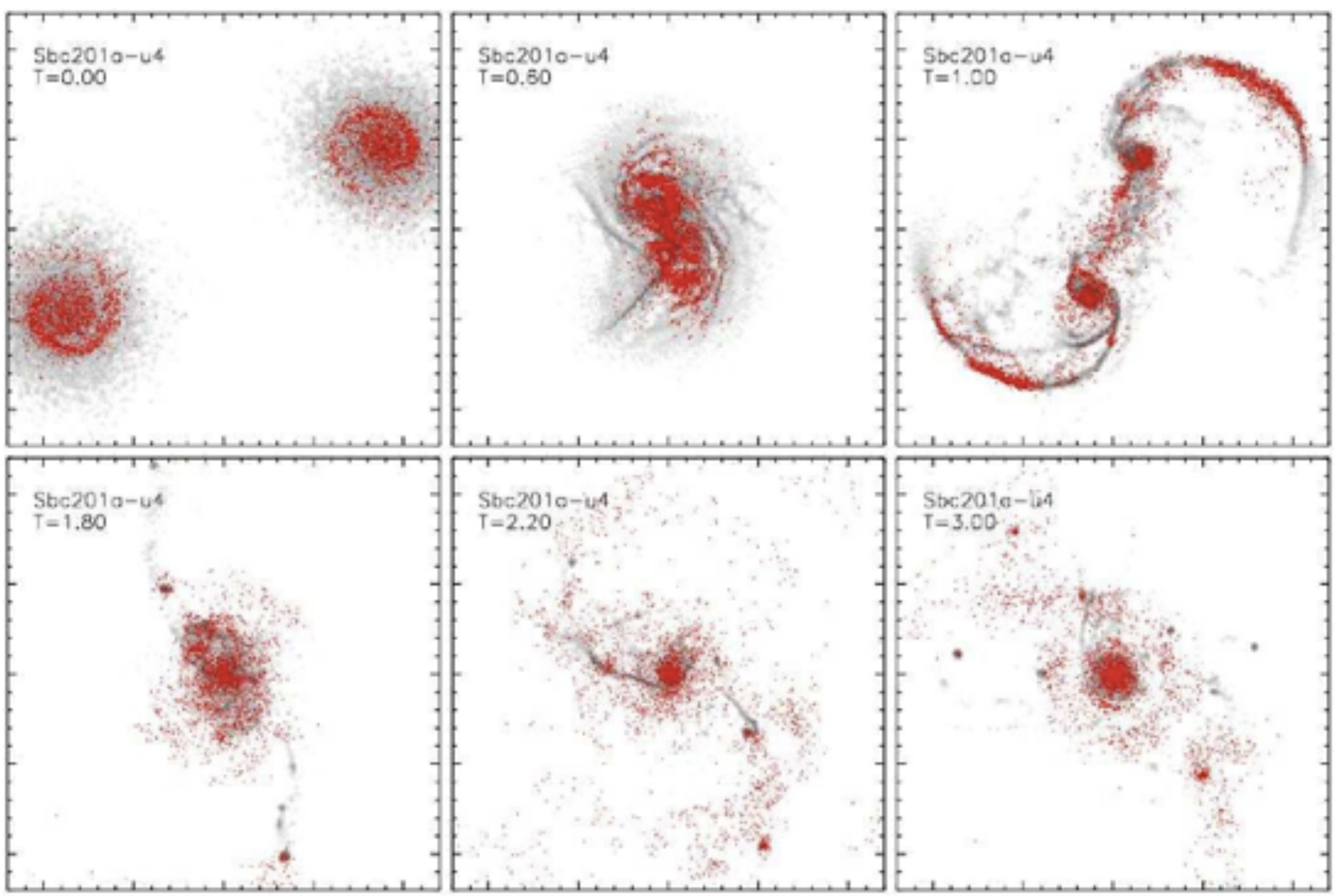

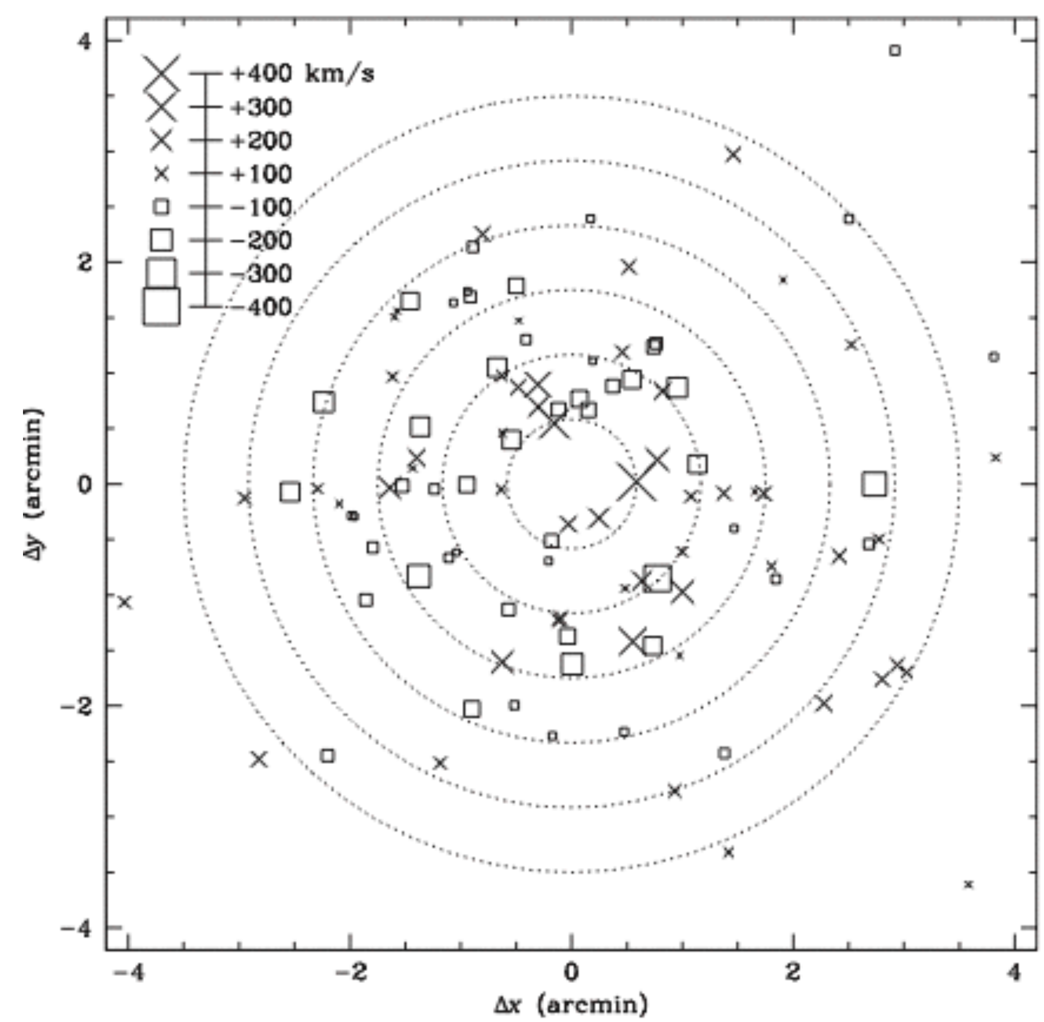

http://adsabs.harvard.edu/abs/2005Natur.437..707D

The dark halo of NGC 3379

Weijmans et al. (2009)

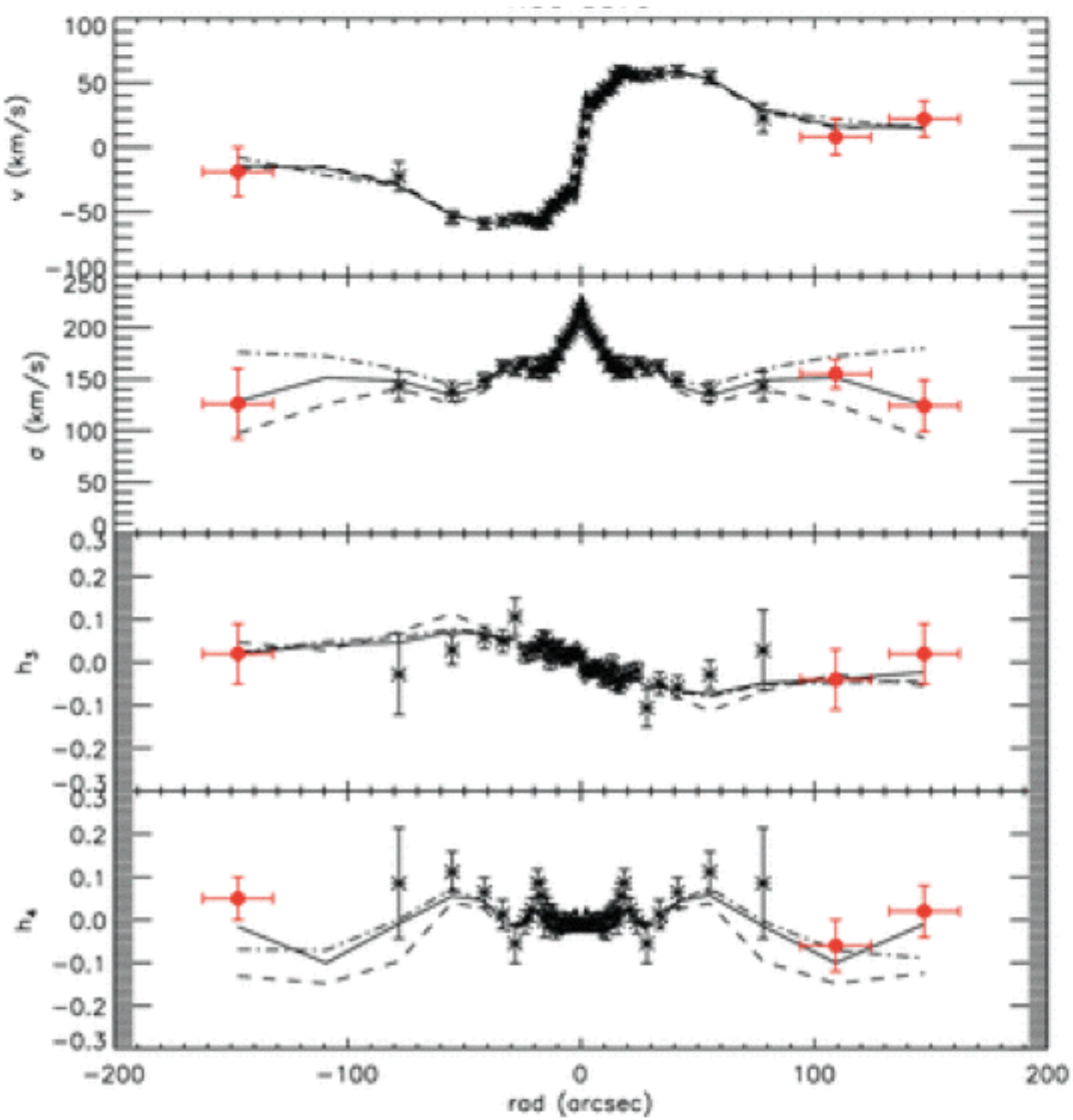

- Solid line → best-fit model
  - $M_{halo} = 1.0 \times 10^{12}\ M_\odot$ = 10 times stellar mass
- Dashed line → model without halo
  - excluded by higher order moments
- Dot-dashed line → too massive halo
  - excluded by dispersion profile and higher order moments

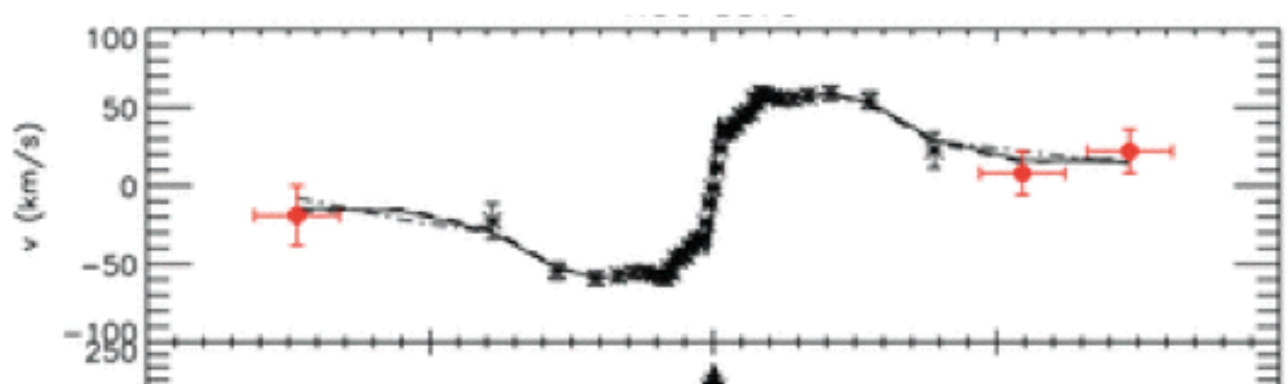

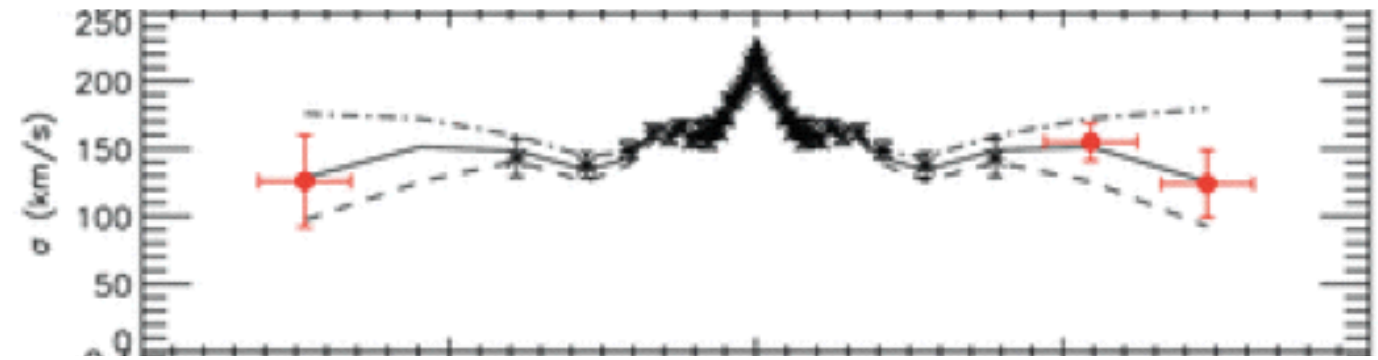

Constrains from the kinematic data

- Observing almost no rotation at large radii
  - need box orbits and/or counter-rotating tube orbits
  - box orbits allowed in triaxial model
- Observing an almost constant dispersion profile
  - potential extra halo mass ‘hides’ on radial orbits
- Observing $h_4 > 0$ at large radii
  - requires radial anisotropy
  - box orbits are OK
  - counter-rotating tube orbits are NOT OK